https://doi.org/10.5194/wes-2025-273
Preprint. Discussion started: 16 December 2025

eawe european academy of wind energy
Open Access WIND ENERGY SCIENCE DISCUSSIONS

Extreme wind speeds in tropical cyclones using parametric models

Paul Renaud[1], Léo Vinour[1,2,3], Fabien Leckler[1], Shogo Uchiyama[4], and Jean-François Filipot[1]

[1]France Energies Marines, 29280 Plouzané, France
[2]Univ Brest, Ifremer, CNRS, IRD, LOPS, 29280 Plouzané, France
[3]Faculty of Environmental Earth Science, Hokkaido University, Sapporo, Japan
[4]RWE Renewables Japan, Tokyo, Japan

Correspondence: Paul Renaud (paul.renaud@france-energies-marines.org)

Abstract. Tropical cyclones are among the most destructive natural disasters. Accurately estimating wind speeds during these extreme weather events remains a challenge, but is essential for optimising the design of offshore structures, such as offshore wind turbines, which could be exposed to such phenomena. In this paper, a state-of-the-art parametric model fed with the best-track dataset is implemented to predict wind generated by tropical cyclones at hub height. The surface wind model accounts for a parametric axisymmetric surface wind model and an asymmetric part, being both adjusted on satellite-borne Synthetic Aperture Radar observations. The surface wind is then extrapolated vertically with a logarithmic law using the WASP drag coefficient. The performance of this extrapolation is first assessed with wind measurements of five tropical cyclones. Then, modelled wind time series and surface wind fields are compared with measurements and high-fidelity models. The consistent results confirm the ability of the model to predict extreme tropical cyclone winds. A key limitation of parametric models lies in their omission of large-scale orographic effects, as illustrated by the complex terrain of Taiwan.

1 Introduction

The offshore wind industry targets areas exposed to tropical cyclones (TC), such as the Asia Pacific or the United States East Coast. Because they are rare events, statistics based on historical datasets are not very reliable and may be subject to considerable uncertainty. Thus, risk assessment is usually based on statistical approaches where a larger number of synthetic events is created. Synthetic tracks are generated using Monte Carlo-type approaches from a genesis location (Vickery et al., 2000; Emanuel et al., 2006; Kim and Lee, 2019; Bloemendaal et al., 2020) or for site-specific location (Vickery and Twisdale, 1995; Ishihara and Yamaguchi, 2015; Wang et al., 2022). These methods predict wind speeds with parametric wind models (see Yan and Zhang, 2022, for a review) using the synthetic TC characteristic parameters from a probability distribution fitted on a best-track dataset. Another method is to apply a parametric wind model to a best-track dataset and derive wind statistics from extreme value theory (Ott, 2005). With only a few input parameters, an easy implementation and a low computational cost, parametric models have been extensively used for both TC wind risk assessment and wave models forcing (e.g. Grossmann-Matheson et al., 2023).

Recent advances in high-resolution remote sensing technology enable accurate observations of TC winds (Mouche et al., 2019). Building on such innovations, Vinour et al. (2025) fitted parameters of axisymmetric and asymmetric parametric wind

https://doi.org/10.5194/wes-2025-273
Preprint. Discussion started: 16 December 2025

eawe european academy of wind energy
Open Access WIND ENERGY SCIENCE DISCUSSIONS

models on synthetic aperture radar (SAR) surface wind field measurements. The best axisymmetric model is the model from Loridan et al. (2015) which uses the latitude (ϕ), the maximum wind speed (V_m) and the radius of maximum wind (R_m) as input parameters. Vinour et al. (2025) also calibrated the input parameters of the asymmetric wind model from Olfateh et al. (2017) using V_m, R_m and the TC translation speed C as parameters for the multi-linear regressions.

The International Best Track Archive for Climate Stewardship (IBTrACS) (Knapp et al., 2010, 2023), which unifies observational estimates of TC main characteristics from a wide range of meteorological agencies, provides the input parameters listed above to feed the parametric models to estimate wind speeds at a given site. IBTrACS aggregates estimates of TC characteristic parameters (track, minimum pressure and maximum wind, characteristic radii, notably) provided by various meteorological agencies worldwide. Those estimates are carried out by each agency individually, by analysing and harmonising a range of different observational sources, including satellite measurements and aircraft observations. The inherent limitations of each type of observation, combined with the gathering of heterogeneous datasets across agencies, result in large uncertainties in parameter estimates. In particular, the estimation of R_m remains uncertain, as this quantity is difficult to measure and is poorly resolved numerically (Chavas and Knaff, 2022). This can lead to significant discrepancies in estimating wind speed using parametric models (Avenas et al., 2023). Alternatively, R_m can be estimated from other TC parameters using empirical adjustment as proposed in Willoughby and Rahn (2004); Chavas and Knaff (2022); Avenas et al. (2023).

For offshore wind turbine design, the extreme wind speed at hub height is required. Consequently, surface wind speed must be extrapolated up to a few hundred meters (e.g. $\approx 200\,\mathrm{m}$ for a 25MW offshore wind turbine (Escalera et al., 2022)). Common practice (IEC, 2019) suggests using a power law following the model from Meng et al. (1997) used in Ishihara and Yamaguchi (2015). The shear exponent is set to 0.10 for offshore conditions, a value commonly found in the literature (Hsu et al., 1994; Türk et al., 2008; Kapoor et al., 2020; Yan et al., 2022). In Giammanco et al. (2012), power laws are fitted to dropsonde wind speed measurements collected in hurricanes in open sea conditions. Values of shear exponent between 0.06 and 0.10 are reported. Shear exponent is also numerically assessed in Müller et al. (2024a), where median values lower than IEC recommendations are found. The vertical wind distribution in TC can also be evaluated using logarithmic profiles (Powell et al., 2003; Vickery et al., 2009; Mudd and Vickery, 2025) that relate the friction of the atmospheric flow on the ocean surface to the vertical variation of wind speed through parameters such as the friction velocity and the roughness length. This model requires the evaluation of the drag coefficient C_d. Assessing C_d with the contributions of air-sea interactions remains an active field of research, especially for very high speeds since observations are rare and scattered (see Bryant and Akbar (2016) for a review). For offshore wind farm design applications in TC conditions, Ma et al. (2021) and Larsén and Ott (2022) used a drag coefficient varying with surface wind speed U_{10}. In Ma et al. (2021), the gradient wind speed is extrapolated at hub height (100 m) using several formulations, some of which assume a strictly increasing drag coefficient. However, observations suggest a saturation or decrease of drag in strong winds (Powell et al., 2003; Vickery et al., 2009; Bell et al., 2012; Holthuijsen et al., 2012; Hsu et al., 2017) driven by several physical air-sea interaction processes (e.g. air-flow separation at the crest of breaking waves and sea sprays contribution to wind momentum loss) (Bouin et al., 2024). Larsén and Ott (2022) implemented the variable drag coefficient used in the wave model SWAN (Zijlema et al., 2012). The formulation is a second-order polynomial predicting negative C_d for extreme winds ($>69\,\mathrm{m.s^{-1}}$), resulting in inconsistent wind profiles for hurricanes of category 5 on the Saffir-

https://doi.org/10.5194/wes-2025-273
Preprint. Discussion started: 16 December 2025

eawe european academy of wind energy
Open Access WIND ENERGY SCIENCE DISCUSSIONS

Simpson scale (Simpson and Saffir, 1974). It is essential to provide reliable formulas applicable for all intensities, including the most severe ones, since intense tropical cyclones may appear more often in the future (Knutson et al., 2020; Bloemendaal et al., 2020; Emanuel, 2021). Therefore, extrapolating the surface wind to hub height in tropical cyclones using a logarithmic law requires a more consistent description of the variation of the drag coefficient in extreme winds. DNV (2025) proposes a capped formulation of the drag coefficient as a function of the surface wind speed, accounting for a constant C_d of 2.30×10^{-3} for $U_{10} > 27.85\,\mathrm{m.s^{-1}}$. The recent parameterisation from Bouin et al. (2024) is also a practical solution to obtain a reasonable variation in C_d as it is based on TC observations for extreme winds. The latter authors propose a wave-age-dependent stress parameterisation (WASP) that provides a mean adjustment over various TC events and assumes a constant drag coefficient of 1.56×10^{-3} for surface wind speeds above $45\,\mathrm{m.s^{-1}}$.

The present study is part of the OROWSHI (Offshore wind turbine design including joint wind-wave information in standards for hurricane-exposed sites) project which aims to better characterise extreme wind and waves statistics to optimise the design of offshore wind turbines (OWT) exposed to TCs. This research effort evaluates the performance of a parametric wind model applied to the best-track parameters to reconstruct historical winds. The parametric wind models are described in section 2. One relies on the model from Vinour et al. (2025) for the surface wind, with parameters adjusted using SAR wind measurements. A second parametric model, based on the gradient wind formulation implemented in Ishihara and Yamaguchi (2015), is also presented. High-fidelity wind models are also used for comparison. The IBTrACS dataset and parameters processing are presented in section 3. Section 4 introduces the location of the sites and the available measurements used as a reference for the performance assessment. The ability of the WASP drag coefficient to extrapolate the surface wind is assessed in section 5. Shear exponents of power laws are also examined. Finally, comparisons between the models and the measurement are presented for five TCs in section 6, including discussions on the results, in particular on the large-scale orographic effects.

2 Wind models

This section presents the wind models that are compared to in situ measurements. First, the two parametric models are described. One is based on a surface wind model, while the second is based on a gradient wind model. The weather forecast model and reanalyses are also presented.

2.1 OROWSHI parametric wind model

2.1.1 Axisymmetric wind model

In Vinour et al. (2025), parametric surface wind models are fitted to SAR observations. Ten parameterisations are proposed and the best regressed model is the one proposed by Loridan et al. (2015). The surface wind field V_s is given by:

$$V_s(r) = \begin{cases} V_0 + (V_m - V_0)\left(\frac{r}{R_m}\right)^n \exp\left[\left(n - \frac{R_m}{X_1}\right)\left(1 - \frac{r}{R_m}\right)\right] & ; r \leq R_m \\ V_m \exp\left(-\frac{r - R_m}{X_1}\left(\frac{r}{R_m}\right)^{Y_1}\right) & ; r > R_m \end{cases} \quad (1)$$

https://doi.org/10.5194/wes-2025-273
Preprint. Discussion started: 16 December 2025

eawe european academy of wind energy
Open Access WIND ENERGY SCIENCE DISCUSSIONS

with $V_0 = V(r = 0)$. The profile is adjustable by fitting the parameters V_0, n, X_1 and Y_1 to surface wind data. The parameters are expressed as functions of the V_m (maximum wind speed), R_m (radius of maximum wind) and ϕ (latitude):

$$p = \alpha_0 + \alpha_1 V_m + \alpha_2 \ln(R_m) + \alpha_3 |\phi| \tag{2}$$

Table 1 presents the coefficients of the multi-linear regression obtained by Vinour et al. (2025).

Table 1. Results of the least-squares regression of the Loridan et al. (2015) model parameters, as given by Vinour et al. (2025).

Parameter	$\boldsymbol{\alpha_0}$	$\boldsymbol{\alpha_2}$	$\boldsymbol{\alpha_3}$	$\boldsymbol{\alpha_4}$
V_0	9.94	9.77×10^{-2}	-1.16	1.61×10^{-2}
$\ln(X_1)$	1.44	9.30×10^{-3}	9.28×10^{-1}	1.10×10^{-2}
$\ln(-Y_1)$	5.10×10^{-1}	-8.20×10^{-3}	-3.41×10^{-1}	1.20×10^{-3}
$\ln(n)$	1.59	1.54×10^{-2}	-2.27×10^{-1}	-2.40×10^{-3}

2.1.2 Asymmetric wind model

The asymmetric wind field V_{as} is given by the formulation from Olfateh et al. (2017) with parameters also fitted on SAR dataset by Vinour et al. (2025). The asymmetric wind V_{as} is given by:

$$V_{as}(r) = \epsilon V_m \sin(\theta + \Phi) \left[e \left(\frac{R_a}{r} \right)^D e^{-\left(\frac{R_a}{r}\right)^D} \right]^{1/2} \tag{3}$$

where θ is the azimuth in the TC reference frame centred on the TC direction of propagation. R_a is the distance to the maximum wind speed, D is the sharpness of the wind field, ϵ is the asymmetry parameter and Φ is the azimuthal location of the maximum wind speed in the TC reference frame. The parameters are fitted on the same SAR dataset using a multi-linear regression of the parameters R_m, V_m and C (translation speed) (Vinour et al., 2025).

The parameters are expressed as:

$$p = \alpha_0 + \alpha_1 V_m + \alpha_2 \ln(R_m) + \alpha_3 C \tag{4}$$

The coefficients are gathered in Table 2.

The azimuthal location of the maximum wind Φ is defined by a parameterised sectionally continuous linear profile depending on the normalised distance from the TC centre, r/R_m:

$$\Phi(r) = \begin{cases} min(156.1 - 185.6 \frac{r}{R_m}, 0) & ; r/R_m < r_c \\ -54.1 - 3.5 \frac{r}{R_m} & ; r/R_m \geq r_c \end{cases} \tag{5}$$

https://doi.org/10.5194/wes-2025-273
Preprint. Discussion started: 16 December 2025

eawe european academy of wind energy
Open Access WIND ENERGY SCIENCE DISCUSSIONS

Table 2. Results of the least-square regression of the asymmetric wind model parameters.

Parameter	α_0	α_2	α_3	α_4
ϵ	3.50×10^{-1}	-2.89×10^{-3}	-3.00×10^{-2}	8.30×10^{-3}
$\ln(R_a)$	5.91×10^{-1}	-1.50×10^{-2}	9.26×10^{-1}	4.92×10^{-2}
D	9.30×10^{-1}	-4.16×10^{-3}	2.55×10^{-1}	-2.37×10^{-2}

with r_c = 1.154.

The asymmetric wind is added to the axisymmetric wind given by Eq. 1 to obtain the total surface wind.

2.2 Vertical extrapolation

The surface wind model provides the wind field at 10 m above the sea level. However, for OWT design, wind speed at hub height (e.g. between 100 m and 200 m, depending on the OWT power) is required. To do so, the surface wind is extrapolated using a logarithmic law assuming a neutral atmosphere:

$$U(z) = \frac{u^*}{\kappa} \ln\left(\frac{z}{z_0}\right) \tag{6}$$

with u^* the friction velocity, κ the von Kármán constant (= 0.4) and z_0 the roughness length. The friction velocity is related to the surface shear through the drag coefficient C_d:

$$\tau = \rho {u^*}^2 = \rho C_d U_{10}^2 \tag{7}$$

with ρ the air density and U_{10} the mean wind speed at 10 m above sea level.

The drag coefficient obtained from the WASP parameterisation (Bouin et al., 2024) is used in the present study. It provides a mean value among experimental data in TC conditions. Figure 1 displays its variation with the surface wind U_{10} as well as the formulation used in Ma et al. (2021); the SWAN formula employed in Larsén and Ott (2022) and the formulation recommended by DNV (2025).

In section 5, the accuracy of the logarithmic profile using the WASP drag coefficient is assessed with vertical wind profile measurements.

2.3 Local orographic effects

The upstream orography may disturb the wind flow. A standard practice for accounting for these effects is to compute a speed-up ratio that corrects the wind from the parametric model (Ishihara et al., 2005; Ishihara and Yamaguchi, 2015). The speed-up ratio is defined as the ratio between the wind computed over the actual orography and the wind speed over a flat surface of

https://doi.org/10.5194/wes-2025-273
Preprint. Discussion started: 16 December 2025

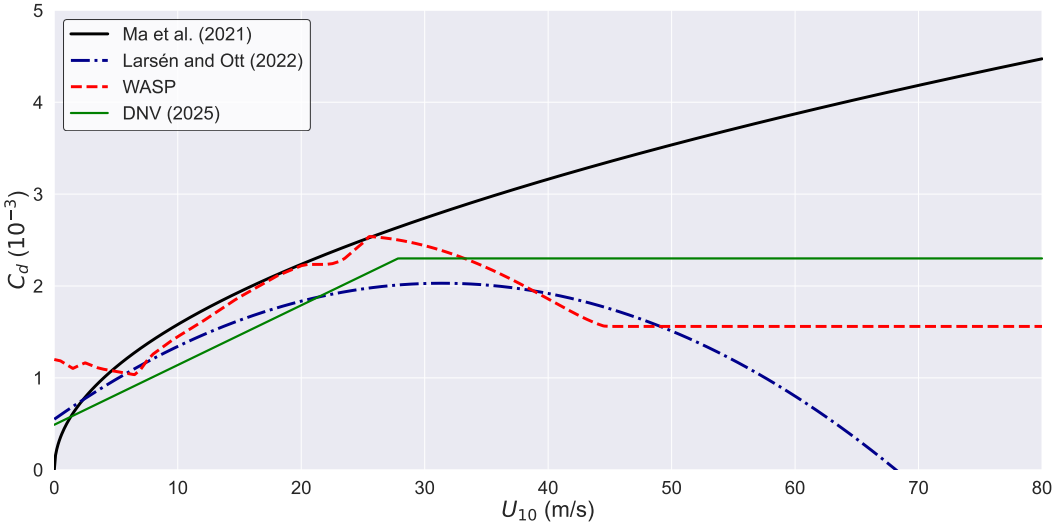

Figure 1. Drag coefficient as a function of surface wind speed U_{10} for various parameterisations.

uniform roughness. The MASCOT[1] software (Ishihara and Hibi, 2002) is used to derive the variation of the speed-up ratio with wind direction. Here, a constant inflow angle of -22.5° (Powell et al., 2009; Zhang and Uhlhorn, 2012; Tamizi et al., 2020) is considered to determine the actual wind direction. The speed-up ratio is applied to the surface wind, before the vertical extrapolation.

2.4 Ishihara and Yamaguchi (2015) wind model (I&Y15)

For comparison, the wind model described in Ishihara and Yamaguchi (2015) (referred to in IEC (2019)) is implemented. The model relies on the gradient wind formula from Meng et al. (1995), which assumes that the pressure gradient force, given by Schloemer (1954)'s formulation, is balanced by the centrifugal and Coriolis forces. The gradient wind is then extrapolated to the altitude of interest using a power law (Meng et al., 1997). Ishihara and Yamaguchi (2015) considered a shear exponent of 0.1 for offshore applications. The shear exponent depends on the roughness length through an empirical formula in Ishihara and Yamaguchi (2015). For wind over terrain, the Global Land Cover dataset from Copernicus (Buchhorn et al., 2020) gives a 100-m resolution discrete classification of the type of soil. Each class is assigned a roughness length. The roughness length over sea is set to 0.00016 m to match a shear exponent of 0.1 using the empirical formulation from Ishihara and Yamaguchi (2015). Land effects are accounted for by using a speed-up ratio, applied to the extrapolated wind speed at the height of interest.

The averaging time of the wind speed from this parametric model applied to the best-track dataset is a 3-hour average (U_{3h}) (Yasui et al., 2002). Yasui et al. (2002) proposed to model the difference between 3-hour and 10-min wind speed as a normal distribution with a standard deviation that follows:

[1]MASCOT User's Manual (in Japanese), 6th ed., AQUANET Corporation, Japan, 2023

https://doi.org/10.5194/wes-2025-273
Preprint. Discussion started: 16 December 2025

eawe european academy of wind energy
Open Access WIND ENERGY SCIENCE DISCUSSIONS

$$\sigma_u = 0.1 U_{3h} \tag{8}$$

The 10-min wind time series is obtained by adding random values following a normal distribution to the 3-hour average.

Morever, in the following, comparisons of surface wind fields are presented. The 10-min wind field is derived from the 3-hour wind field by using the time conversion model described in Yamaguchi et al. (2012). The maximum M minutes average wind speed U_M^{max} to 10-min average U_{10-min}^{max} is computed from:

$$\frac{U_M^{max}}{U_{10-min}^{max}} = 1 - 0.0810\left(\frac{M-10}{60}\right)^{0.5457} \tag{9}$$

With M = 180, the conversion factor is 0.857.

2.5 High-fidelity wind models

For comparison, high-fidelity models accounting for more physics are presented. Below is a brief description of the available data.

2.5.1 Wind fields from the Hurricane Weather Research and Forecasting Model - HWRF

The Hurricane Weather Research and Forecasting (HWRF) model from NOAA (National Oceanic and Atmospheric Administration) is a mesoscale, ocean-coupled numerical weather prediction model designed specifically for tropical cyclone forecasting (Biswas, 2018). The data used in this study consists of wind fields provided at a resolution of 0.015° (0.02° for events prior to 2018). HWRF is initialised either through data assimilation or using a bogus vortex approach. The model solves the non-hydrostatic Reynolds-Averaged Navier–Stokes equations over time using the WRF model (Janjic, 2004), producing forecasts at 3-hour or 6-hour intervals. To minimise forecast errors and model drift from observations, only the first forecast outputs at 3-hour and 6-hour lead times are used in this study. Vertical profiles are provided at isobaric levels, with the first level corresponding to surface winds (10 m above mean sea level). The second level is derived using the hypsometric equation:

$$z_2 = (\ln P_1 - \ln P_2)\left(\frac{R}{g}T\right) \tag{10}$$

with P_1 = 1000 hPa (first level), P_2=975 m (second level), R is the specific gas constant , g is the acceleration of gravity and T is the air temperature (K).

In this study, HWRF wind fields are treated as 10-min averaged winds. Although the model output does not explicitly specify the temporal averaging period, winds from mesoscale numerical weather prediction models, such as HWRF, correspond to time-averaged values rather than instantaneous gusts due to numerical filtering and space averaging (Harper et al., 2010). This assumption is supported by the model's use of parameterised subgrid turbulence and boundary-layer schemes, which inherently smooth high-frequency variability. Therefore, for consistency with the averaging time of the observations used in this study, HWRF winds are assumed to represent 10-min averaged values.

https://doi.org/10.5194/wes-2025-273
Preprint. Discussion started: 16 December 2025

eawe european academy of wind energy
Open Access WIND ENERGY SCIENCE DISCUSSIONS

2.5.2 Wind fields from the European Centre for Medium-Range Weather Forecasts reanalysis version 5 - ERA5

The European Centre for Medium-Range Weather Forecasts reanalysis version 5 (ERA5) (Hersbach et al., 2023) uses data assimilation of observations and weather models to provide hourly estimates of atmospheric parameters on a horizontal grid of resolution 0.25° since 1940. Wind speeds at 10 m and 100 m are extracted during the cyclonic events. The measurements presented in this study are 10-min wind speeds. The hourly wind estimates are converted to 10-min wind using Eq. 9 with M = 60.

2.5.3 Vertical extrapolation

In this study, the wind speed is assessed at a representative hub height of an offshore wind turbine, from $\approx$ 100 m to 200 m depending on the data available.

Since only two levels are considered for HWRF and ERA5, a power law is used to extrapolate the wind speed at the desired altitude:

$$U(z) = U_{10}\left(\frac{z}{10}\right)^{\alpha} \tag{11}$$

with α the shear exponent, computed from the wind speeds at the two available altitudes:

$$\alpha = \frac{\ln U(z_2) - \ln(U_{10})}{\ln z_2 - \ln 10} \tag{12}$$

$U(z_2)$ is the wind speed at the second altitude, z_2, corresponding to 100 m for ERA5 and $\approx$ 220 m for HWRF (T $\approx$ 300 K for all time steps of the cases presented in the following).

3 IBTrACS data processing

The IBTrACS dataset provides TC locations and characteristic parameters at a 3-hour time step that are used by the present model (OROWSHI) and by the model of Ishihara and Yamaguchi (2015) (I&Y15) presented previously. First, the locations of the TC are interpolated at 10-min intervals using quadratic splines. The translation direction is derived from the interpolated locations. The TC characteristic parameters from the US agency are linearly interpolated along the tracks. However, the raw parameters provided by IBTrACS do not exactly correspond to the input of the parametric model. For example, the maximum sustained wind speed and the radius of maximum wind are two-dimensional (e.g. estimated from the pixel of maximum wind on a SAR image), while the two parametric models, OROWSHI and I&Y15 require azimuthally averaged values (one-dimensional). The processing of the TC parameters provided by IBTrACS is presented below.

https://doi.org/10.5194/wes-2025-273
Preprint. Discussion started: 16 December 2025

eawe european academy of wind energy
Open Access WIND ENERGY SCIENCE DISCUSSIONS

3.1 Maximum wind speed

The maximum wind speed from IBTrACS is local (2D) while the axisymmetric wind profile from Loridan et al. (2015) requires an azimuthally averaged V_m. In this study, the correction proposed by Vinour et al. (2025) is implemented to obtain an azimuthal average maximum wind, consistent with the parametric model. The relationship follows:

$$V_m = 0.8066 V_{IBTrACS} + 2.985 \tag{13}$$

with $V_{IBTRrACS}$ corresponding to the parameter USA_WIND in the dataset.

3.2 Wind speed averaging period conversion

The surface wind model presented in section 2.1 is based on SAR measurements, which are assumed 1-min wind speeds. This is also the reference averaging period of V_m provided by the US agency (Knapp et al., 2010). Bloemendaal et al. (2020) applied a conversion factor of 0.88 to align V_m at 10-min while Reul et al. (2016) and Meissner et al. (2017) used 0.93 as recommended by Harper et al. (2010). The value of 0.93 is also adopted in the present study. Note that Eq. 9 is not valid for $M < 10$, hence the use of this conversion factor.

3.3 Radius of maximum wind

Chavas and Knaff (2022) highlighted that R_m is difficult to measure and is badly resolved in models and reanalyses. Here, R_m is estimated from V_m, ϕ and R_{34} following the methodology from Chavas and Knaff (2022). The angular momentum is given by

$$M_a = rV + \frac{1}{2} f r^2 \tag{14}$$

with r the radius, V the tangential wind speed and f is the Coriolis parameter.

Knowing the ratio $M_a(r = R_{max})/M_a(r = R_{34})$, R_m can be computed as follows:

$$R_m = \frac{V_m}{f}\left(\sqrt{1 + \frac{2 f M_{a_{max}}}{V_m^2}} - 1\right) \tag{15}$$

Avenas et al. (2023) computed the ratio $M_a(r = R_{max})/M_a(r = R_{34})$ from a SAR-radiometer collocation dataset and derived the following parameterisation, adopted here:

$$M_{a_{max}}/M_{a34} = 0.531 \exp\left[-0.00214(V_m - 17.5) - 0.00314(V_m - 17.5)(\frac{1}{2} f R_{34})\right] \tag{16}$$

In the IBTrACS dataset, R_{34} is available for the TC four quadrants. The mean value of R_{34} is used to consistently obtain an axisymmetrical R_m.

https://doi.org/10.5194/wes-2025-273
Preprint. Discussion started: 16 December 2025

eawe european academy of wind energy
Open Access WIND ENERGY SCIENCE DISCUSSIONS

The parameterisation (Eq. 16) was obtained with a 1-min azimuthally averaged wind speed. The V_m from IBTrACS corrected by Eq. 13 is used to estimate R_m in Eq. 15 and 16.

In Ishihara and Yamaguchi (2015), R_m is fitted from measured sea surface pressure, but no pressure measurements are available on the site of this study. Since Schloemer (1954) equation is an axisymmetric pressure model which requires an azimuthal average R_m, R_m obtained from the abovementioned methodology is used. Note that the current implementation differs from the original study from Ishihara and Yamaguchi (2015) as parameters from the Japan Meteorological Agency (JMA) were used, restricting the application to the Western Pacific basin. In particular, R_m is not provided by the JMA. In this study, the TC parameters from the US agency are used. Since they are provided for almost every TC, the current implementation is applicable anywhere.

3.4 Pressure

The I&Y15 model requires the ambient pressure for the Schloemer (1954) model, taken to 1013 hPa (IEC, 2019) here. The USA_PRES parameter from the IBTrACS dataset gives the central pressure, which is used to quantify the central pressure depth.

4 Site description

4.1 Japan

A lidar located at 33.70°N, 129.62°E recorded winds from Typhoon Hinnamnor & Nanmandol (2022) on 20 vertical levels from 50 m to 285 m. Only measurements at 95 m and 205 m are considered for comparison with wind models. The locations of the TCs provided by IBTrACS are represented in Fig. 2. The wind intensity V_m from the US agency is presented for each location. The minimum distance from the TC centre to the site is 2.8 R_m and 1.0 R_m for Typhoon Hinnamnor and Nanmandol, respectively.

The site is relatively close to Iki Island ($\approx$ 5 km). Thus, local orographic effects may affect the wind. The variation of the speed-up ratio with wind direction (True North convention) is presented in Fig. 3. The decrease in wind direction between 0 and 90° is due to Iki Island while Kyushu Island affects the wind speed from 90° to 225°.

4.2 New York Bight

A floating lidar located at 39.55°N, 73.43°W recorded the winds of Hurricane Isaias (2020). Figure 4 displays the TC track and wind intensity. The TC passed about 2.0 R_m from the site. During the event, two of the four quadrants of the TC are overland, with values of R_{34} very low compared to those over sea. Since the present study aims at evaluating the performance of the parametric models over the sea, only the mean R_{34} of the eastern quadrants is used for this case. The vertical discretisation of the measurements is 20 m from 18 m to 198 m. The altitudes 98 m and 198 m are used as reference for the comparison of the wind speed.

https://doi.org/10.5194/wes-2025-273
Preprint. Discussion started: 16 December 2025

eawe european academy of wind energy
Open Access WIND ENERGY SCIENCE DISCUSSIONS

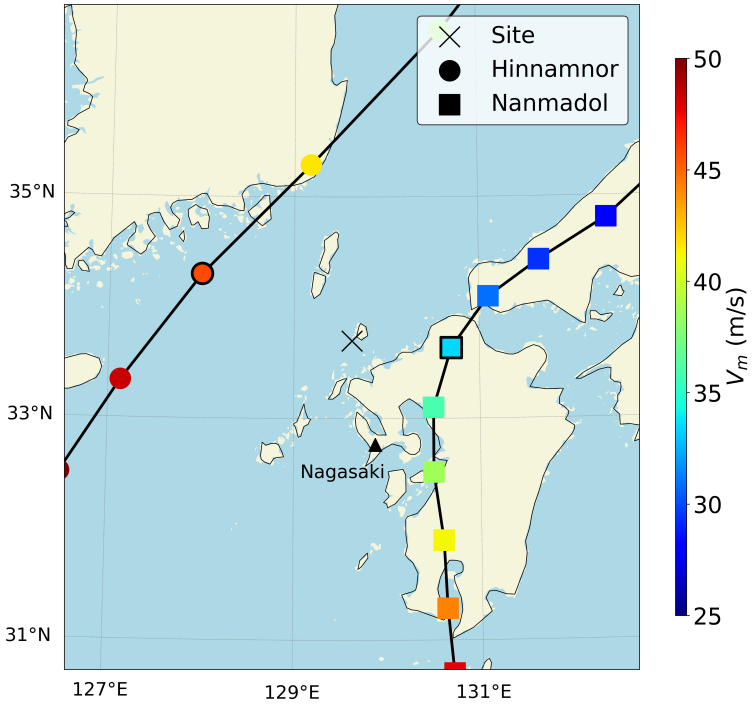

Figure 2. Measurement site (X) impacted by Typhoon Hinnamnor (●) & Nanmadol (■) (both in 2022). The black outline on the marker highlights the location closest to the site.

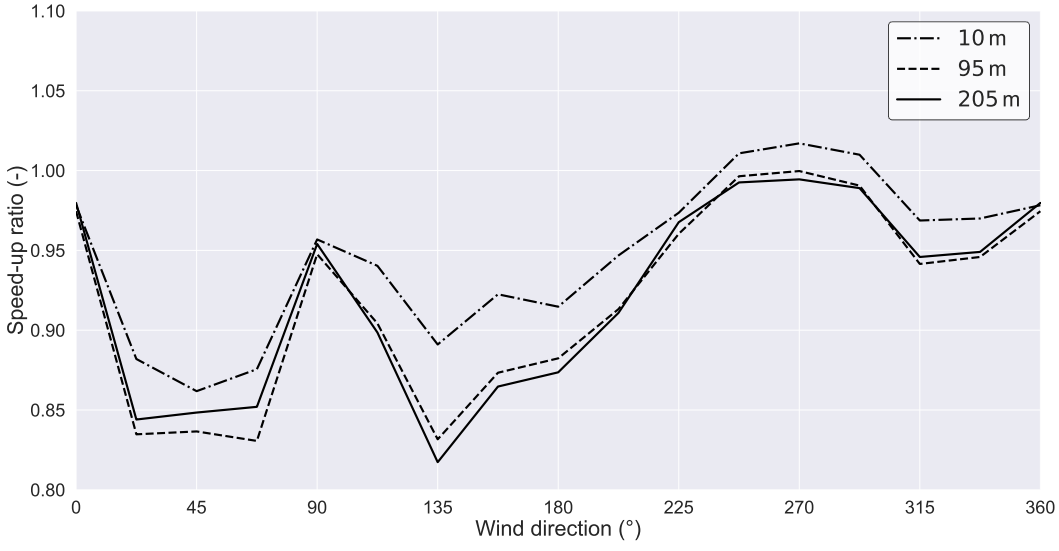

Figure 3. Variation of the speed-up ratio with wind direction at 10 m, 95 m and 205 m above the mean sea level.

https://doi.org/10.5194/wes-2025-273
Preprint. Discussion started: 16 December 2025

eawe european academy of wind energy
Open Access WIND ENERGY SCIENCE DISCUSSIONS

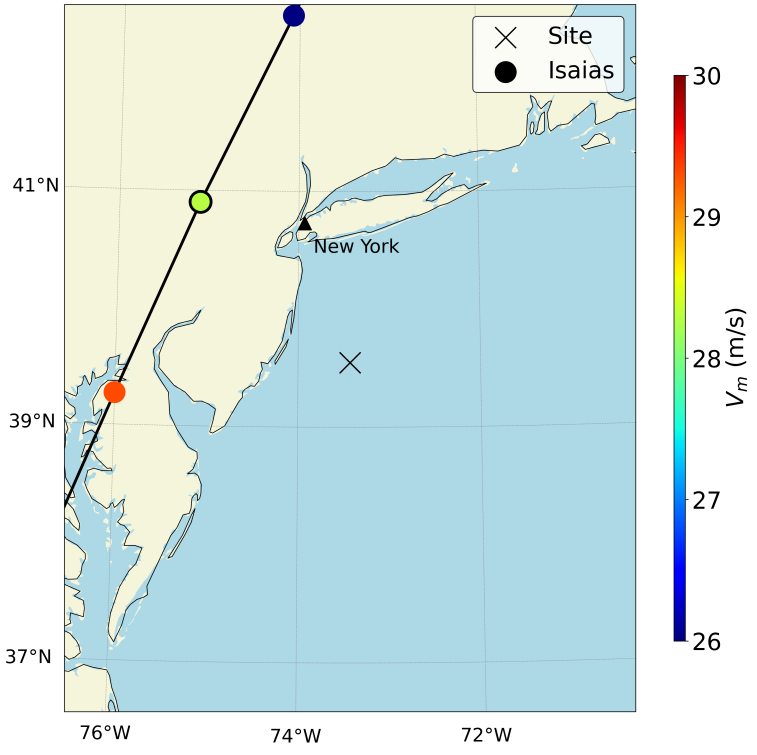

Figure 4. Measurement site (X) impacted by Hurricane Isaias (●) (2020).

The site is over 60 km from the coast. In this case, orographic effects are neglected.

4.3 Taiwan

Taiwan is hit by numerous typhoons every year. With mountains over 3 km high, this island is of particular interest for studying the interactions of tropical cyclones with mesoscale orography (e.g. Wu et al., 2015; Tang and Chan, 2016; Hsu et al., 2018; Müller et al., 2024a).

4.3.1 Site 1

The metmast is located offshore at 24.71°N, 120.83°E. The tracks of TC Dujuan (2015) and Megi (2016) are presented in Fig. 4. The minimum distance of Dujuan from the site is 1.6 R_m and 1.0 R_m for Megi. Measurements are available from 30 m to 90 m, equally spaced by 20 m.

4.3.2 Site 2

The measurement tower is located at 25.04°N, 121.07°E. There are 5 measurement levels from 50 m to 105 m. Winds from TC Megi (2016) were recorded. Estimating a speed-up ratio to account for local orographic effects is challenging for such a large

https://doi.org/10.5194/wes-2025-273
Preprint. Discussion started: 16 December 2025

eawe european academy of wind energy
Open Access WIND ENERGY SCIENCE DISCUSSIONS

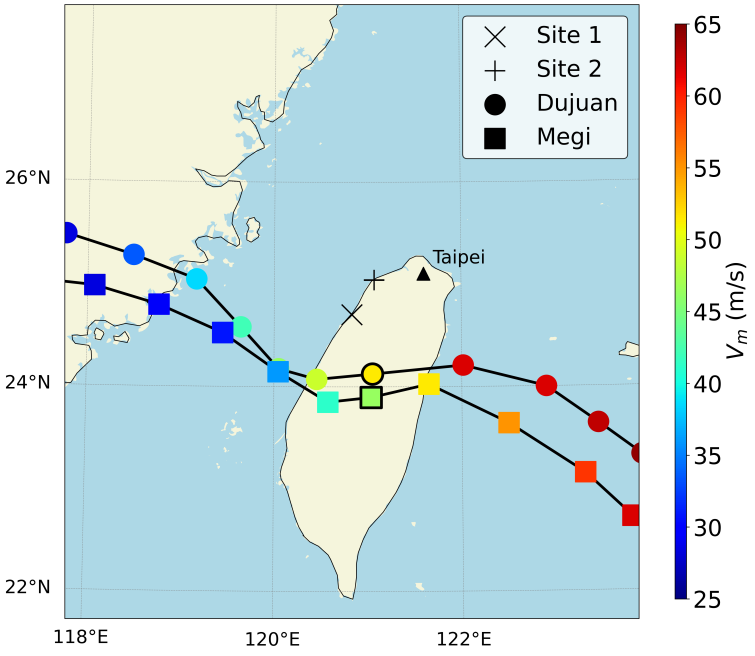

Figure 5. Measurement sites impacted by Typhoon Dujuan (sites: X & + , track: ●) (2015) & Megi (site: +, track: ■) (2016).

island as Taiwan. Indeed, the domain size is usually a few 10 km within MASCOT, which is enough when evaluating the flow over a relatively low orography, such as in the site studied in Ishihara and Yamaguchi (2015), characterised by rather close, low-lying, and small-scale orographic obstacles. Wind flow over large mountain islands, such as Taiwan, is disturbed on a much larger scale, and the whole TC structure is affected. CFD cannot give reliable results in such cases. There are alternatives to CFD for taking orographic effects into account, such as design codes, e.g. British Standards Institution (2005) used in Tan and Fang (2018), but Taiwan is also outside the scope of these methods. Consequently, orographic effects are not taken into account in these cases.

5 Application - Vertical extrapolation

This section presents the assessment of the vertical wind distribution. First, the logarithmic law and the WASP drag coefficient are evaluated and compared to the measurements. Then, the shear exponent of the power law is derived. Only strong wind events ($U_{10} > 25\,\mathrm{m.s^{-1}}$) are analysed to not account for wave growth and keep only cyclonic events.

5.1 Assessment of the logarithmic law

The surface wind speed and the drag coefficient are derived from a least-squares linear fitting as in Powell et al. (2003) for each sample. u^*/κ is given by the slope and z_0 by the intercept on a log height scale. The surface wind U_{10} is derived from Eq. 6

https://doi.org/10.5194/wes-2025-273
Preprint. Discussion started: 16 December 2025

eawe european academy of wind energy
Open Access WIND ENERGY SCIENCE DISCUSSIONS

and the drag coefficient from Eq. 7. Figure 6 displays the drag coefficient computed for each sample from the 10-min mean wind speed. The observations are highly scattered and site-dependent. The drag coefficient derived from TC Megi (2016) is significantly different depending on the site, with a ratio of 2 between the two sites for $U_{10} > 30\,\mathrm{m.s^{-1}}$. This discrepancy may be attributed either to upstream topographic effects or to differences in wave conditions within the Taiwan Strait. The WASP and DNV (2025) formulations are presented for comparison. The two parameterisations are consistent with the mean value, which does not vary substantially for this wind speed range. Table 3 presents the Mean Bias Error (MBE) and Root Mean Square Error (RMSE) computed at 200 m (corresponding to hub height of 25 MW OWT (Escalera et al., 2022)) using WASP drag coefficient and DNV's recommendations. The reference value is computed from the fitted log law since level 200 m is not available in the data. The lowest errors are obtained with WASP. Extreme wind speeds at hub height are thus better estimated on average using the WASP drag coefficient than the DNV recommendation for this dataset.

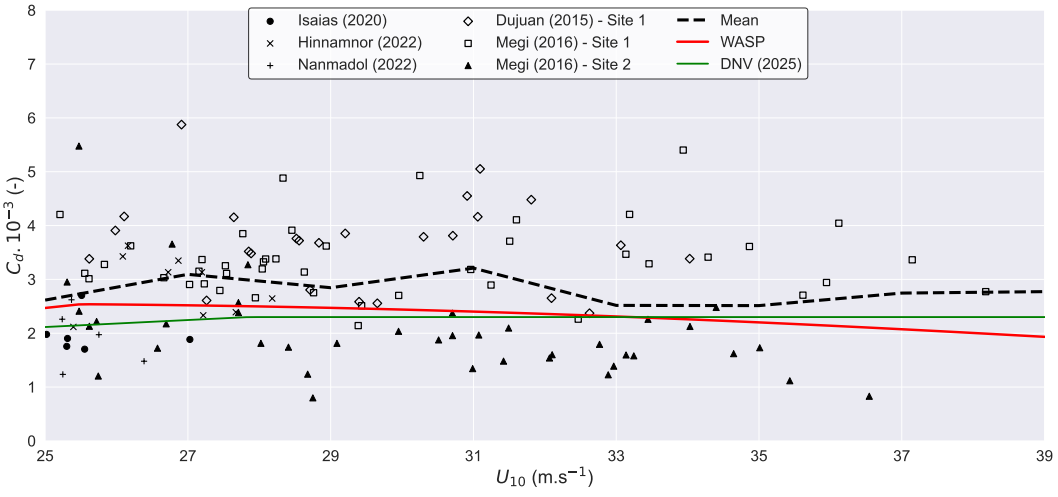

Figure 6. Drag coefficient as a function of surface wind U_{10}. Comparison between WASP, DNV (2025) and the measurements. The black dashed line corresponds to the mean measured value for bins of $2\,\mathrm{m.s^{-1}}$.

Table 3. Scores at 200 m using log laws.

Model	MBE ($\mathrm{m.s^{-1}}$)	RMSE ($\mathrm{m.s^{-1}}$)
DNV (2025)	-6.3	6.4
WASP	-0.7	2.3

5.2 Assessment of the power law

The power law (Eq. 11) is also widely used in the industry to extrapolate wind speed. DNV (2025) suggests using an exponent α = 0.12 for open sea conditions with waves. In Ishihara and Yamaguchi (2015), α is set to 0.10. Recommendations from

https://doi.org/10.5194/wes-2025-273
Preprint. Discussion started: 16 December 2025

eawe european academy of wind energy
Open Access WIND ENERGY SCIENCE DISCUSSIONS

IEC (2019) suggest extrapolating the 50-year extreme wind speeds using α = 0.11. The shear exponent is derived from the measurement to assess the reliability of the various proposed values.

A power law is fitted to the vertical profiles with U_{10} and shear exponent α as free parameters. Figure 7 presents the variation of the shear exponent with the surface wind. There is no significant variation of the mean value of α as a function of U_{10}, which is equal to 0.106. The median is 0.107, slightly higher than the value reported in Müller et al. (2024a). Table 4 presents the MBE and RMSE computed at 200 m using shear exponents from 0.10 to 0.12. IEC's recommendations give the best results for this dataset. Although the power law with a shear exponent $\alpha = 0.11$ performs slightly better, the logarithmic law based on the WASP drag coefficient is retained for its stronger physical basis and interpretability.

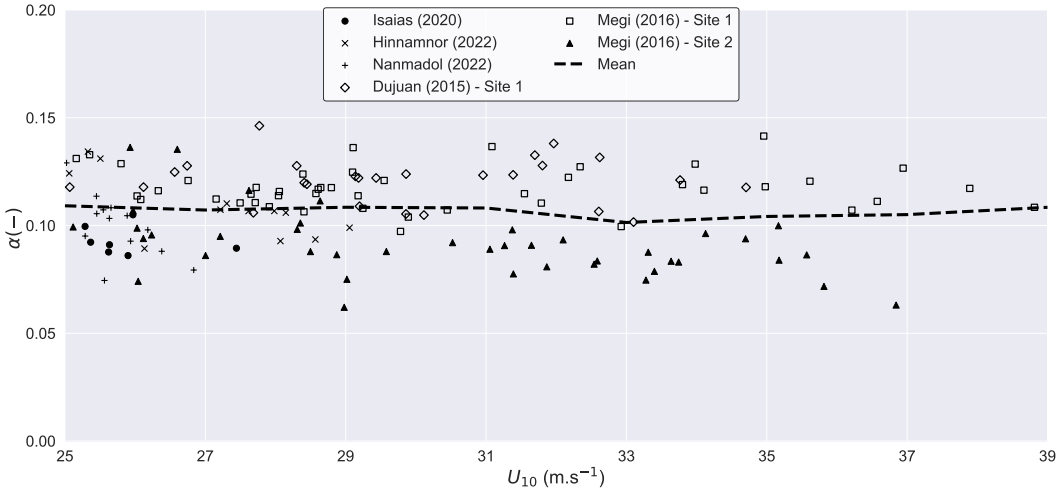

Figure 7. Wind shear exponent α as a function of surface wind U_{10}.

Table 4. Scores at 200 m using power laws.

Shear exponent	MBE ($\mathrm{m.s^{-1}}$)	RMSE ($\mathrm{m.s^{-1}}$)
$\alpha = 0.10$	-0.9	2.3
$\alpha = 0.11$	0.3	2.2
$\alpha = 0.12$	1.6	2.7

6 Application - Wind time series

This section compares the wind speeds predicted by the models with the measurements. The MBE and RMSE are computed or each event on the time series of measured 10-min averaged wind speed. Moreover the parametric models are to be used within the framework of a Monte Carlo approach. Generally, straight-line propagation is implemented from the TC location closest to

https://doi.org/10.5194/wes-2025-273
Preprint. Discussion started: 16 December 2025

eawe european academy of wind energy
Open Access WIND ENERGY SCIENCE DISCUSSIONS

the site (Vickery and Twisdale, 1995; Ishihara et al., 2005). In the end, only the maximum wind induced by each TC at the site is used to derive extreme wind statistics. It is therefore necessary to assess the ability of the models to capture the maximum wind at a given site. The percent deviation from the maximum measured wind ($\mathrm{PD}_{\max}$) is thus evaluated. In addition, surface wind fields centred on the best-track location are presented. Note that the HWRF wind field is a forecast. Thus, the TC centre may deviate from the location provided in IBTrACS. The intensity of the storms (two-dimensional maximum surface wind speed) predicted by the models is also discussed. The Bias Error (BE) on the maximum 10-min sustained wind speed is computed using IBTrACS data as a reference.

6.1 Typhoon Hinnamnor (2022)

Wind time series from TC Hinnamnor are presented in Fig. 8. All the methods presented here align well with the observations. The scores of the parametric models are similar to those of the high-fidelity models (see Table 5). The surface wind field estimated by the four models is presented in Fig. 9. Parametric models predict an eyewall spot similar to that of HWRF (Fig. 9a). ERA5 (Fig. 9b) clearly underestimates the inner core but matches the outer core reasonably well due to its accurate representation of weak winds.

The formulation used in Ishihara and Yamaguchi (2015) always predicts the location of the azimuth of maximum wind at 90° on the right-hand side of the forward speed direction (41° here) (Fig. 9d), which is reasonable for this case. However, the area of high wind is larger than that predicted by HWRF and by the OROWSHI model, which could lead to different sea states in this area. The 1-min maximum sustained wind speed provided by the US Agency is $45.8\,\mathrm{m.s}^{-1}$. Applying a conservation factor of 0.93 (Harper et al., 2010), the 10-min wind speed is $42.6\,\mathrm{m.s}^{-1}$. The local maximum wind speeds (2D) from the asymmetric profiles are gathered in Table 6. ERA5 highly underpredicts the wind intensity, due to its coarse horizontal resolution but also to inadequate physics parameterisations for cyclonic conditions (Xu et al., 2024). The parametric models predict well the intensity. Although both models are based on IBTrACS parameters, they differ in their primary inputs: the OROWSHI model is driven by maximum wind speed (Eq. 13), whereas I&Y15 depends on the central pressure depth, leading to discrepancies in V_m estimates.

Table 5. Scores of the wind models for TC Hinnamnor at 95 m and 205 m.

Model	**98 m**			**198 m**		
	MBE ($\mathrm{m.s}^{-1}$)	RMSE ($\mathrm{m.s}^{-1}$)	$\mathrm{PD}_{\max}$ (%)	MBE ($\mathrm{m.s}^{-1}$)	RMSE ($\mathrm{m.s}^{-1}$)	$\mathrm{PD}_{\max}$ (%)
OROWSHI	2.1	3.6	-1.4	1.8	3.4	-1.8
I&Y15	-2.8	4.3	0.5	-3.2	4.6	0.9
ERA5	1.0	2.5	-4.4	1.6	2.9	-0.4
HWRF	2.2	3.6	-5.3	1.9	3.6	-5.6

https://doi.org/10.5194/wes-2025-273
Preprint. Discussion started: 16 December 2025

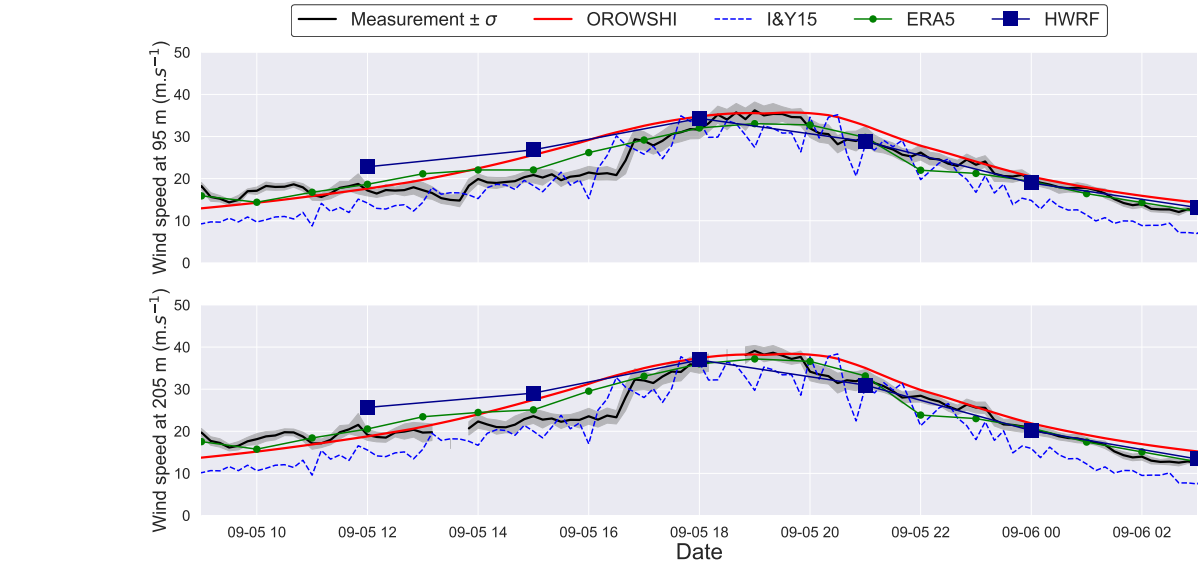

Figure 8. Time series of observed and predicted winds of TC Hinnamnor at 95 m (top panel) and 205 m (bottom panel).

Table 6. Comparison of V_m (2D) and Bias Error between IBTrACS and the models for TC Hinnamnor on 5 September at 6 P.M. GMT.

Model	IBTrACS	OROWSHI	I&Y15	ERA5	HWRF
V_m/BE ($\mathrm{m.s^{-1}}$)	42.6	43.7/1.1	47.1/4.5	30.4/-12.2	51.0/8.4

6.2 Typhoon Nanmadol (2022)

Figure 10 presents the results for TC Nanmadol. The parametric models underestimate the wind speed during the TC approaching phase by a factor of 2, which is a source of large errors in terms of MBE and RMSE (see Table 7). Nevertheless, the peak wind speed and the wind during the leaving phase are quite well predicted. The surface wind fields during the approaching phase are presented in Fig. 11. HWRF results (Fig. 11.a) show that the high-wind spot is at the opposite of the forward speed ($\beta = 357°$ at this instant). The asymmetry is certainly due to the island's blocking action, which can not be represented by the OROWSHI model as it relies on SAR images over open seas. Note that the eyewall predicted by the I&Y15 model is also much larger in this case.

The surface wind fields during landfall on 18 September at 6 P.M. GMT are presented in Fig. 12. The OROWSHI model (Fig. 12.c) is not designed to predict such configurations. The area of high winds predicted by HWRF and by the OROWSHI model is located just around Kyushu Island's northern part, while the surface wind from I&Y15 model is rather axisymmetrical. Table 8 gathers the maximum local wind speeds. Since the parametric models used IBTrACS parameters measured at sea, they accurately estimate the maximum wind speed. At this instant, both HWRF and ERA5 underestimate the intensity.

https://doi.org/10.5194/wes-2025-273
Preprint. Discussion started: 16 December 2025

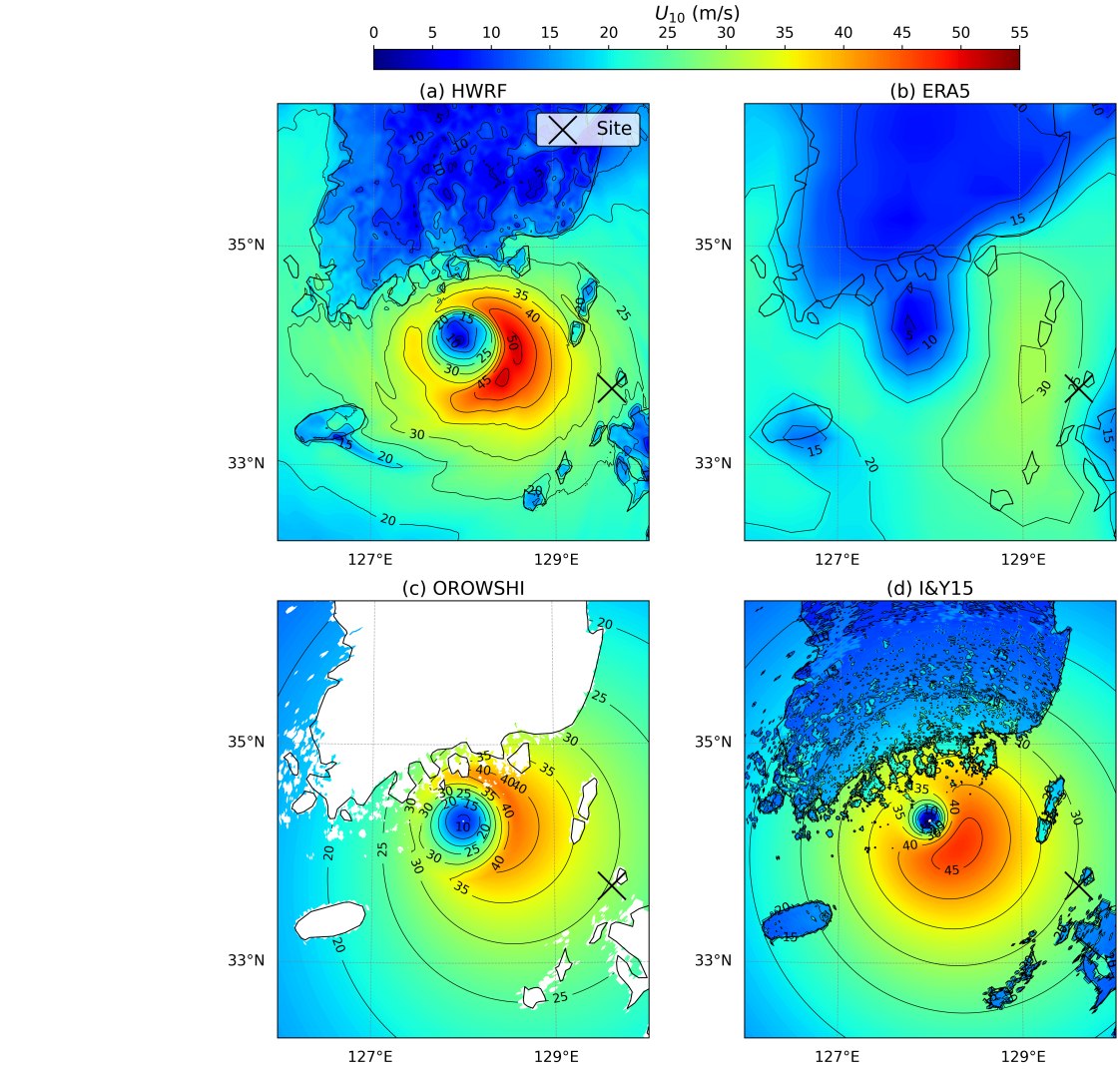

Figure 9. TC Hinnamnor surface wind field on 5 September at 6 P.M. GMT predicted by HWRF (a), ERA5 (b), OROWSHI wind model (c) and I&Y15 wind model (d).

6.3 Hurricane Isaias (2020)

The wind time series of TC Isaias is displayed in Fig. 13. The proposed model shows a reasonable agreement with the measurements with low MBE and RMSE (see Table 9), but all models underestimate the main wind peak. The winds from I&Y15 largely underestimate the measures during the whole event.

https://doi.org/10.5194/wes-2025-273
Preprint. Discussion started: 16 December 2025

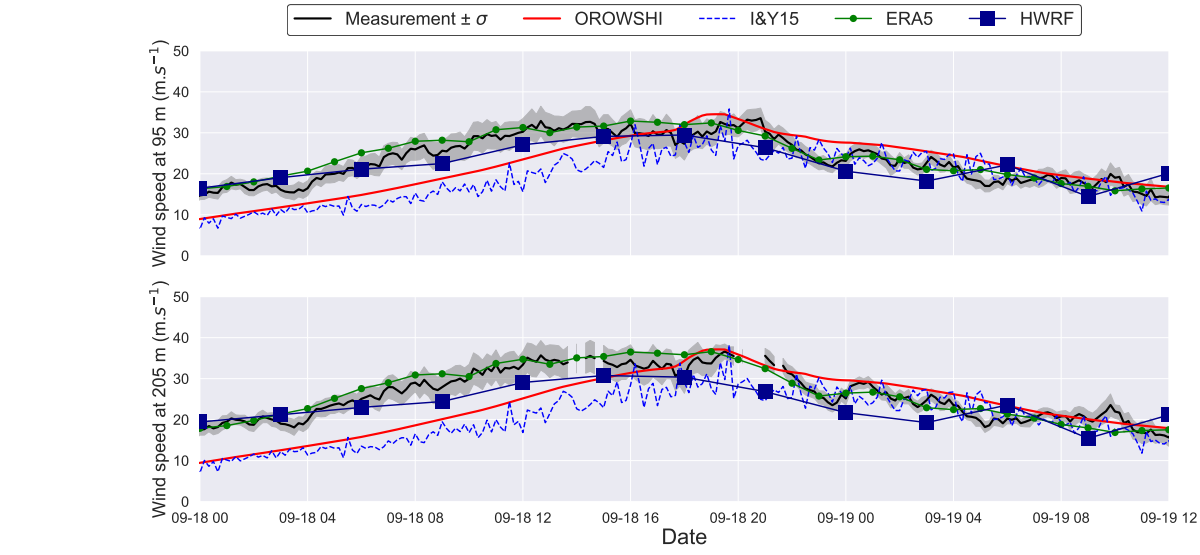

Figure 10. Time series of observed and predicted winds of TC Nanmadol at 95 m (top panel) and 205 m (bottom panel).

Table 7. Scores of the wind models for TC Nanmadol at 95 m and 205 m.

Model	**98 m**			**198 m**		
	MBE ($m.s^{-1}$)	RMSE ($m.s^{-1}$)	PD_{max} (%)	MBE ($m.s^{-1}$)	RMSE ($m.s^{-1}$)	PD_{max} (%)
OROWSHI	-1.4	4.8	2.9	-2.7	5.7	1.3
I&Y15	-4.4	6.8	-3.0	-5.9	8.1	-5.7
ERA5	2.1	2.8	2.6	1.8	2.8	4.6
HWRF	-0.5	3.2	-12.2	-1.8	4.26	-16.1

Figure 14 shows the surface wind field obtained with the four models. The TC had landfall. The high-wind area is above the ocean. The TC intensity (Table 10) is reasonably estimated. The faster decay of the wind profile using the I&Y model causes the TC to have a smaller coverage than the other methods, which explains the wind speed underestimation at the site.

6.4 Typhoon Dujuan (2015) & Megi (2016)

Wind speeds at Taiwan are presented in Fig. 15; 16 & 17. The parametric models can reproduce the increase of the wind until the main peak, but deviate from the measurement during the leaving phase.

The wind direction measured during TC Megi is presented in Fig. 18. The crosses correspond to the instant of maximum wind speed measured at sites 1 and 2. The wind blows from the sea during the main peak (wind direction lower than 30° for site 1 and 70° for site 2). Therefore, neglecting orographic effects has no impact on the maximum speed estimate in this case. Thus, the parametric models fairly captured the main peak with a relatively low PD_{max} (see Table 11; 12; 13). Results from

https://doi.org/10.5194/wes-2025-273
Preprint. Discussion started: 16 December 2025

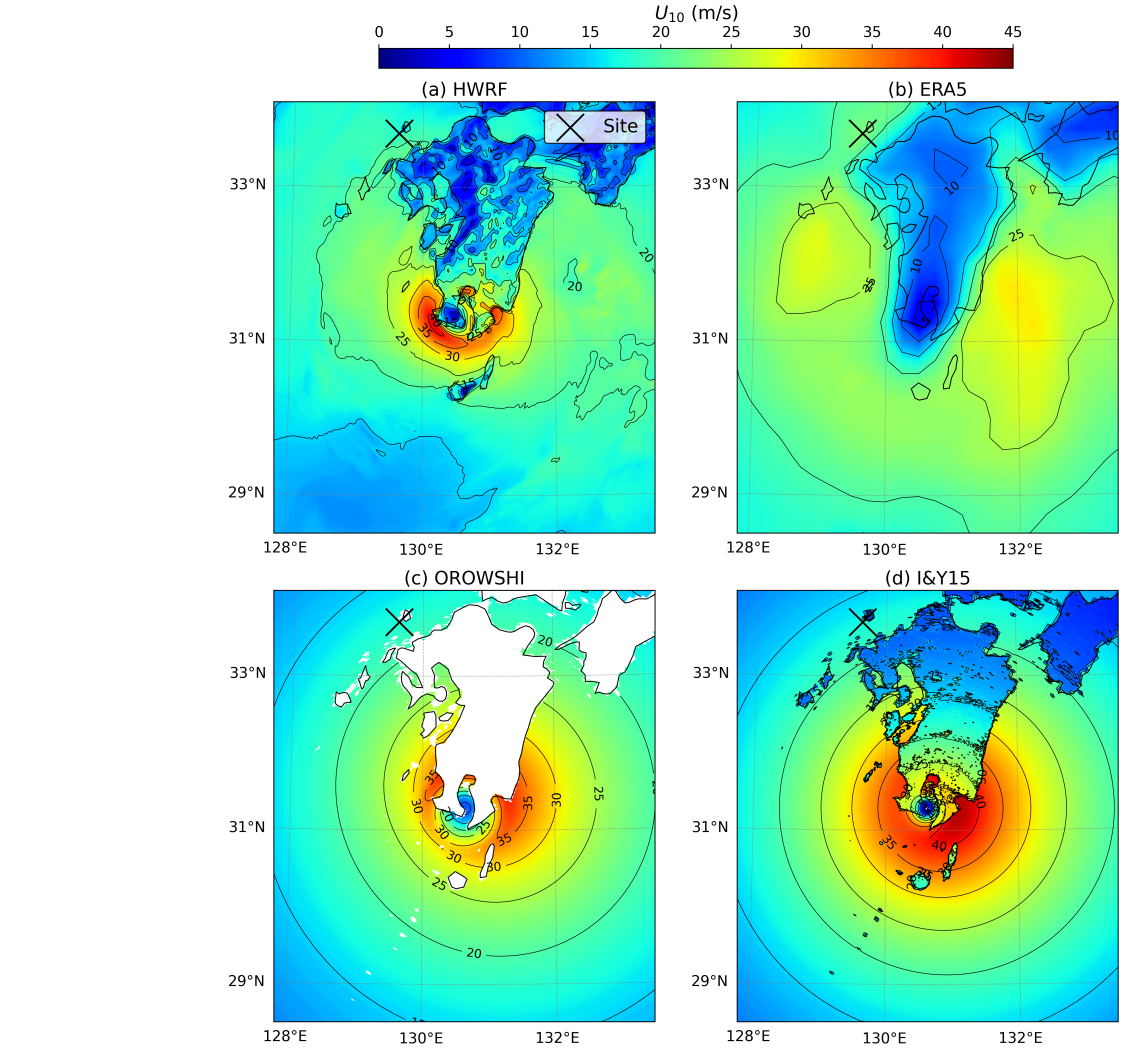

Figure 11. TC Nanmadol surface wind field on 18 September at 9 A.M. GMT predicted by HWRF (a), ERA5 (b), OROWSHI wind model (c) and I&Y15 wind model (d).

Table 8. Comparison of V_m (2D) and Bias Error between IBTrACS and the models for TC Nanmadol on 18 September at 6 P.M. GMT.

Model	IBTrACS	OROWSHI	I&Y15	ERA5	HWRF
V_m/BE ($\mathrm{m.s^{-1}}$)	33.5	33.9/0.4	35.5/2.0	26.5/-7.0	29.4/-4.1

HWRF and ERA5 highly underestimate the maximum wind speeds in these cases. The wind decreases significantly after the main peak as the TC moves to the Taiwan Strait, and the blockage effect due to the islands highly affects the wind prediction.

https://doi.org/10.5194/wes-2025-273
Preprint. Discussion started: 16 December 2025

eawe european academy of wind energy
Open Access WIND ENERGY SCIENCE DISCUSSIONS

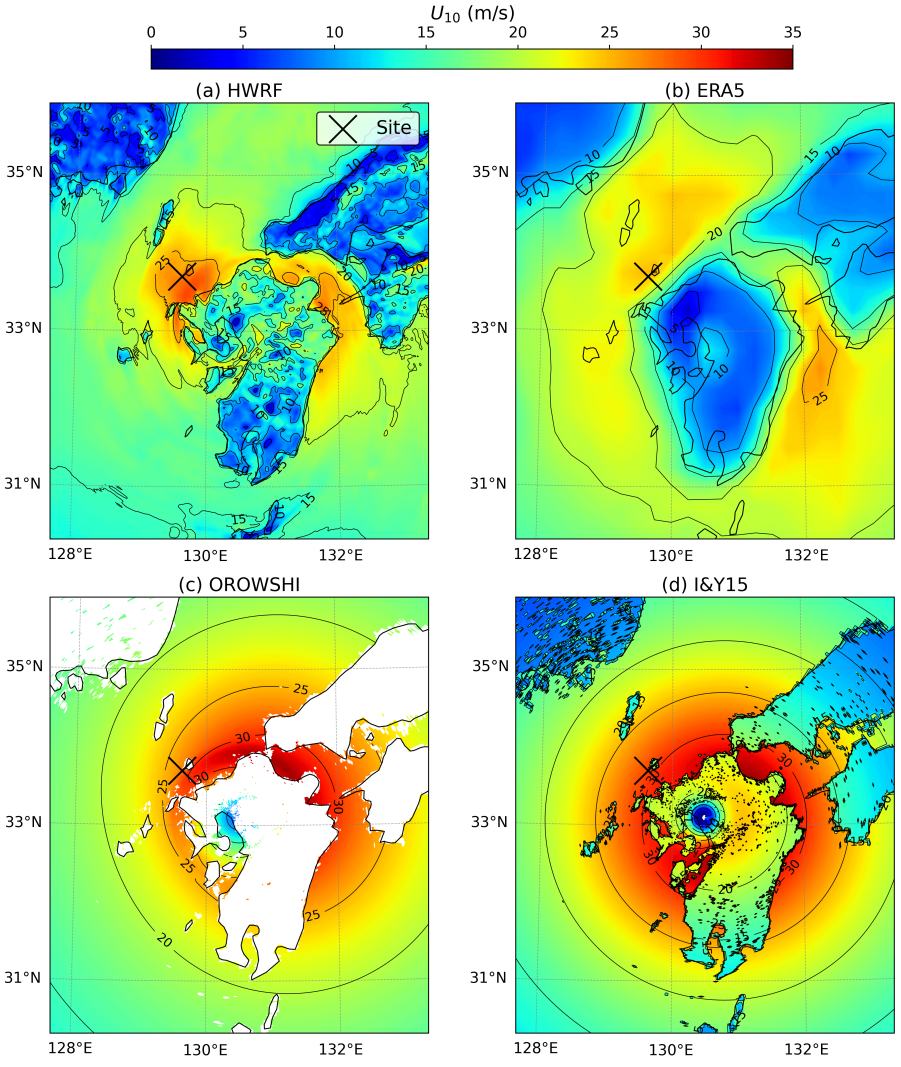

Figure 12. TC Nanmadol surface wind field on 18 September at 6 P.M. GMT predicted by HWRF (a), ERA5 (b), OROWSHI wind model (c) and I&Y15 wind model (d).

As HWRF results are not available for Typhoon Dujuan, the surface wind assessment focuses on Typhoon Megi, which was also studied in Müller et al. (2024b, a) among two similar configurations. The surface wind field of TC Megi on 27 September at 6 A.M. is shown in Fig. 19. The wind field predicted by HWRF (Fig. 19.a) is highly unstructured, while ERA5 (Fig. 19.b) largely underestimates the surface wind around the island. Also, at site 1, the wind speed at the second altitude (222 m) predicted by HWRF is slightly lower than the surface wind, leading to a negative shear exponent (-2.8×10^{-3}). The vertical extrapolation using a power law is thus invalid between the first two levels, while the wind speed increases for vertical

https://doi.org/10.5194/wes-2025-273
Preprint. Discussion started: 16 December 2025

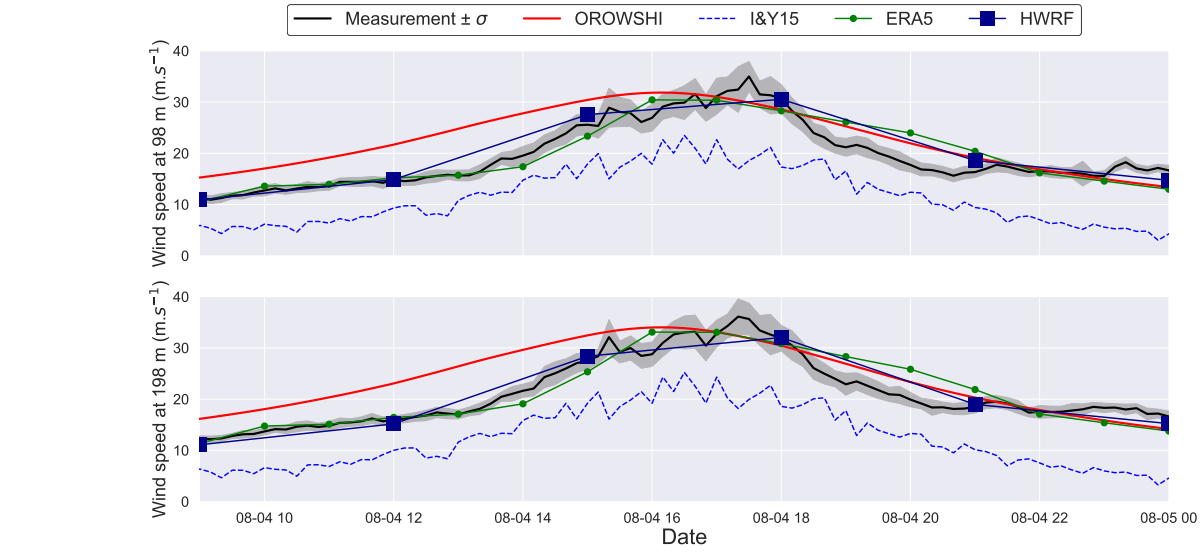

Figure 13. Time series of observed and predicted winds of TC Isaias at 98 m (top panel) and 198 m (bottom panel).

Table 9. Scores of the wind models for TC Isaias at 98 m and 198 m.

Model	**98 m**			**198 m**		
	MBE ($m.s^{-1}$)	RMSE ($m.s^{-1}$)	PD_{max} (%)	MBE ($m.s^{-1}$)	RMSE ($m.s^{-1}$)	PD_{max} (%)
OROWSHI	3.3	4.8	-9.0	3.1	4.7	-5.8
I&Y15	-8.2	8.6	-33.8	-9.0	9.4	-31.1
ERA5	1.4	3.2	-8.9	1.5	3.3	-4.0
HWRF	0.3	1.5	-12.7	-0.3	0.9	-11.3

levels above several hundred meters. ERA5, on the other hand, predicts a shear exponent of 0.173 at the same instant but highly underestimates the observed wind speed.

Due to the presence of the mountains, the eyewalls predicted by both the OROWSHI model (Fig. 19.c) and I&Y15 (Fig. 19.d) are unrealistic, as the parametric models do not account for the orography here. An eyewall positioned on the opposite side of the obstacle (i.e. in the south-eastern quadrant) would be more consistent with HWRF results. Nevertheless, the wind speed in the outer core is fairly predicted and the magnitude of wind speed is reasonably estimated at this instant (see Fig. 16; 17).

The TC intensity is gathered in Table 14. HWRF predicts the highest intensity among the models. However the highest wind on Fig. 19.a might be due to an orographic acceleration over the island (south part of Taiwan).

When the TC moves through the Taiwan Strait, the wind direction increases (Fig. 18) and the wind speed sharply decreases (Fig. 16; 17). The measurement zone becomes very calm with low wind speeds due to the mountain blockage. This is also reported in Müller et al. (2024b), where wind shear and veer vary highly in this area. Large variations in wind direction occur

https://doi.org/10.5194/wes-2025-273
Preprint. Discussion started: 16 December 2025

eawe european academy of wind energy
Open Access WIND ENERGY SCIENCE DISCUSSIONS

Table 10. Comparison of V_m (2D) and Bias Error between IBTrACS and the models for TC Isaias on 8 August at 3 P.M. GMT.

Model	IBTrACS	OROWSHI	I&Y15	ERA5	HWRF
V_m/BE ($\mathrm{m.s^{-1}}$)	27.3	28.3/1.0	30.7/3.4	26.8/-0.5	30.9/3.6

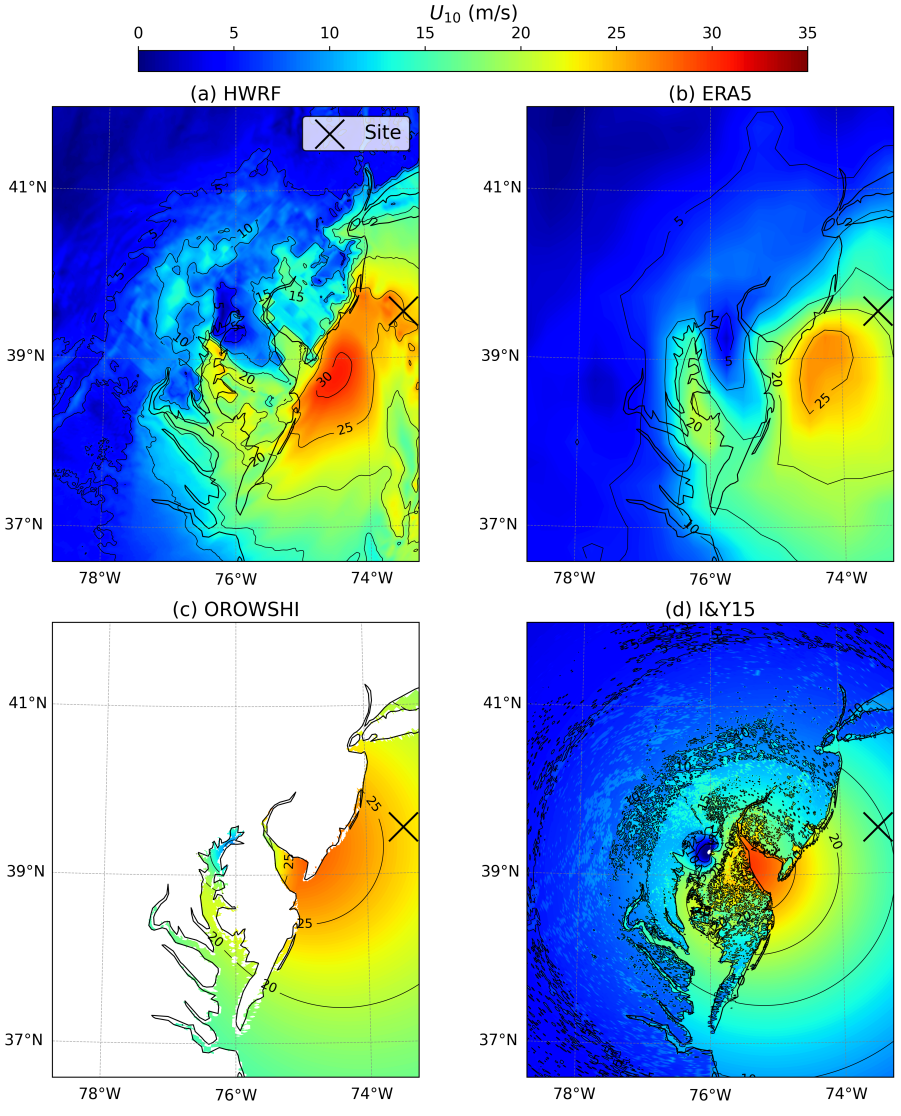

Figure 14. TC Isaias surface wind field on 8 August at 3 P.M. GMT predicted by HWRF (a), ERA5 (b), OROWSHI wind model (c) and I&Y15 wind model (d).

https://doi.org/10.5194/wes-2025-273
Preprint. Discussion started: 16 December 2025

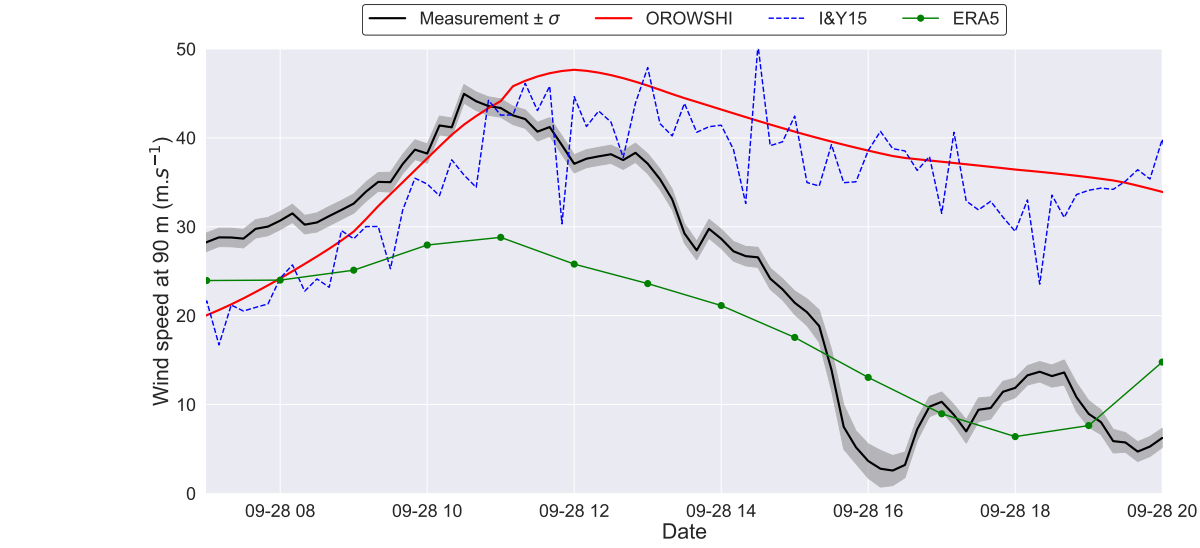

Figure 15. Time series of observed and predicted winds of TC Dujuan at 90 m (site 1).

Table 11. Scores of the wind models for TC Dujuan at 90 m (site 1).

Model	MBE ($\mathrm{m.s^{-1}}$)	RMSE ($\mathrm{m.s^{-1}}$)	$\mathrm{PD_{max}}$ (%)
OROWSHI	13.8	19.5	8.4
I&Y15	10.5	17.6	13.0
ERA5	-4.5	8.2	-34.8

at low wind speeds (see Fig. 16; 17; 18). Parametric models largely overestimate wind at these instants by neglecting orography effects. Thus, the MBE and RMSE for the two parametric models are much higher than in the other configurations (Table 11; 12; 13). HWRF and ERA5 can predict this phenomenon better as they incorporate the effect influence of the terrain. This is illustrated in Fig. 20 where the wind field of the four models is displayed for TC Megi on 27 August at 6 P.M. The TC translation direction is 299°. HWRF can capture fine features due to its high resolution, including orographic acceleration and deceleration, both on the continent and on Taiwan. But the most important is a wake effect on the northwest of the island, at the location of the sites, which is due to the upstream mountain which highly disturbs the wind flow. This is also predicted by ERA5 despite its coarse resolution (Fig. 20b). Also, the high-fidelity models predict an area of strong winds located over the sea at this instant, between the two obstacles, Taiwan and the continental shelf. This illustrates the complexity of wind forecasting using simplified parametric models that do not account for large-scale disturbances generated by an island like Taiwan.

https://doi.org/10.5194/wes-2025-273
Preprint. Discussion started: 16 December 2025

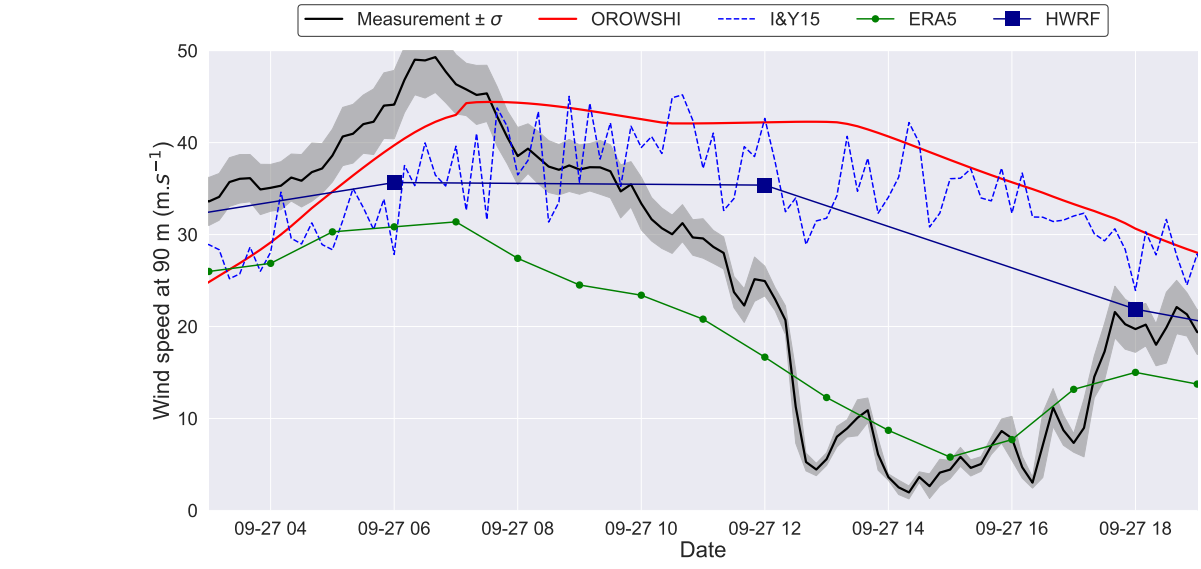

Figure 16. Time series of observed and predicted winds of TC Megi at 90 m (site 1).

Table 12. Scores of the wind models for TC Megi at 90 m (site 1).

Model	MBE (m.s^{-1})	RMSE (m.s^{-1})	$\mathrm{PD}_{\max}$ (%)
OROWSHI	13.6	20.2	-7.8
I&Y15	8.8	17.6	-3.9
ERA5	-6.0	9.1	-38.1
HWRF	1.4	7.9	-27.7

6.5 Synthesis

The mean absolute bias error (MABE), the mean root mean square error (MRMSE) on the wind time series and the mean absolute percentage deviation from the maximum measured wind ($MAPD_{max}$) are presented in Table 15, as well as the mean absolute bias error on the wind intensity in Table 16. The whole time series is better predicted by the high-fidelity models (low MABE and MRMSE) than by the parametric models, which better estimate the highest wind at the sites, an essential parameter for extreme wind statistics. In particular, the OROWSHI model shows only a 5.1% mean absolute percent deviation from the peak observed wind speed, which is less than half the error of the other methods. Also, the wind intensity is well represented by the parametric models, as IBTrACS parameters are used as input for these models. Since the OROWSHI model is forced with the maximum wind speed, its intensity estimates are more accurate than those of I&Y15, which rely on the central pressure depth. The parametric models are highly effective in their field of application, i.e., on the open sea without large-scale disturbances. The source of errors in parametric models is mainly due to land interactions that affect the TC asymmetry, and

https://doi.org/10.5194/wes-2025-273
Preprint. Discussion started: 16 December 2025

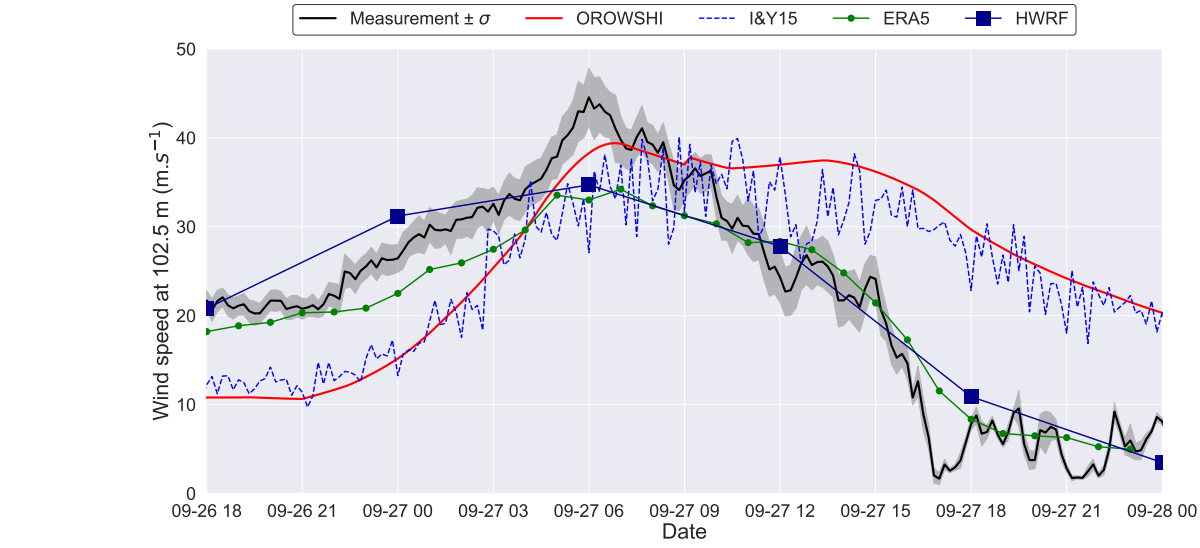

Figure 17. Time series of observed and predicted winds of TC Megi at 102.5 m (site 2).

Table 13. Scores of the wind models for TC Megi at 102.5 m (site 2).

Model	MBE (m.s^{-1})	RMSE (m.s^{-1})	PD_{max} (%)
OROWSHI	5.0	14.3	-7.4
I&Y15	2.6	12.5	-3.6
ERA5	-2.1	4.9	-25.4
HWRF	-0.7	5.2	-22.1

395 orographic effects that strongly decrease wind speed downstream of Taiwan's mountains. In complex environments where tropical cyclones are perturbed at the mesoscale, high-fidelity models are required to capture complex flows. Coupling the ERA5 wind field with a TC parametric model also appears to be a viable approach for improving wind speed predictions under such conditions, as demonstrated by Liu et al. (2025).

https://doi.org/10.5194/wes-2025-273
Preprint. Discussion started: 16 December 2025

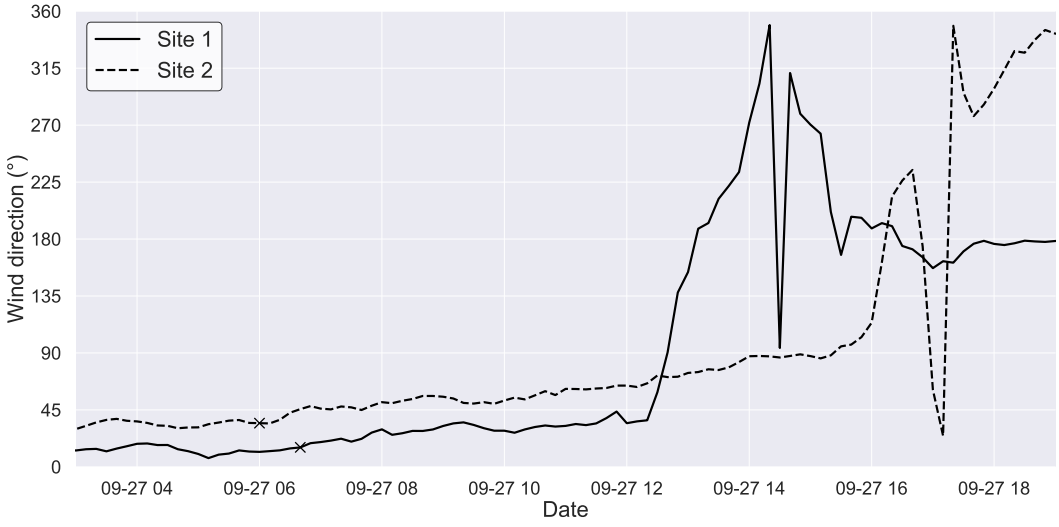

Figure 18. Time series of wind direction during TC Megi at sites 1 and 2. The crosses correspond to the instants of maximum wind speed measured on site.

Table 14. Comparison of V_m (2D) and Bias Error from IBTrACS and predicted by the models for TC Megi on 27 September at 6 A.M. GMT.

Model	IBTrACS	OROWSHI	I&Y15	ERA5	HWRF
V_m/BE $(\mathrm{m.s^{-1}})$	47.8	46.9 / -0.9	46.0 / -1.8	28.9 / -18.9	52.3 / 4.5

7 Conclusions

Tropical cyclone risk assessment mainly relies on the statistical generation of synthetic events to which a parametric wind model is applied. In offshore wind turbine design, the wind speed is extrapolated at hub height. To keep production costs down, and to avoid overly conservative designs due to the uncertainty associated with the lack of knowledge of this extreme phenomenon, reliable and accurate simulation models are essential. This paper is dedicated to the modelling of extreme wind speed in TCs using simplified parametric models that are compared with measurements at relevant altitudes for the offshore wind industry. The model introduced here is based on a surface wind field calibrated on SAR measurements. The wind is vertically extrapolated using a logarithmic law and the WASP drag coefficient. Parameters from the US Agency are used, allowing the model to be applied to any basin. In some cases, local orographic effects are accounted for by using a numerical speed-up ratio. The main aim of this research is to assess the performance of this parametric model at specific sites impacted by tropical cyclones by comparing the wind time series with in-situ observations on one hand, and with more advanced numerical models on the other hand.

Wind measurements of five TC events are analysed to evaluate the performance of the WASP formulation to estimate wind speeds at altitude from surface winds. The drag coefficients obtained from the measurements are scattered but the mean value

https://doi.org/10.5194/wes-2025-273
Preprint. Discussion started: 16 December 2025

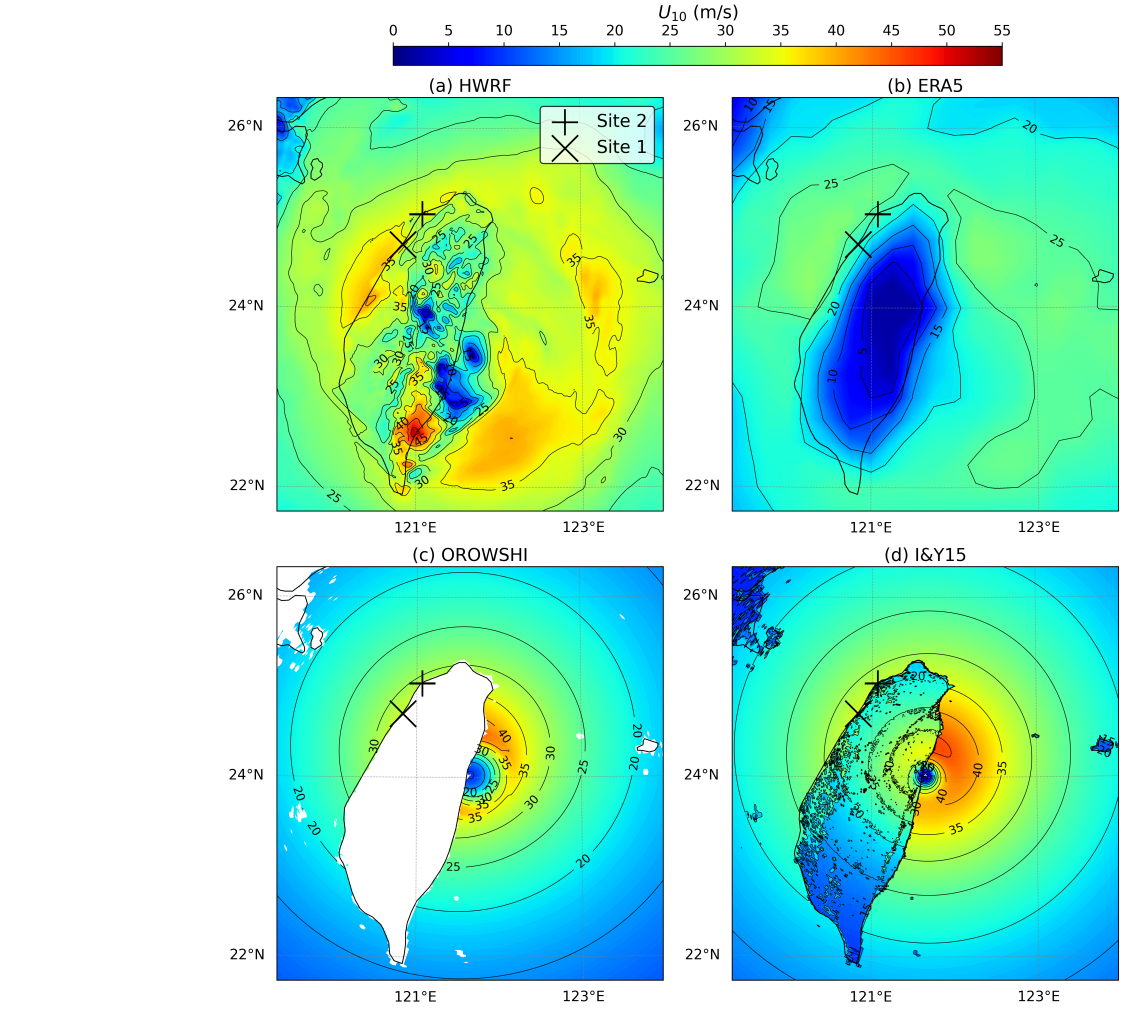

Figure 19. TC Megi surface wind field on 27 September at 6 A.M. GMT predicted by HWRF (a), ERA5 (b), OROWSHI wind model (c) and I&Y15 wind model (d).

Table 15. Mean absolute scores of the wind models.

Model	MABE ($\mathrm{m.s^{-1}}$)	MRMSE ($\mathrm{m.s^{-1}}$)	$\mathrm{MAPD_{max}}$ (%)
OROWSHI	5.2	9.0	5.1
I&Y15	6.1	9.9	10.6
ERA5	1.8	4.1	15.4
HWRF	1.0	3.4	12.6

https://doi.org/10.5194/wes-2025-273
Preprint. Discussion started: 16 December 2025

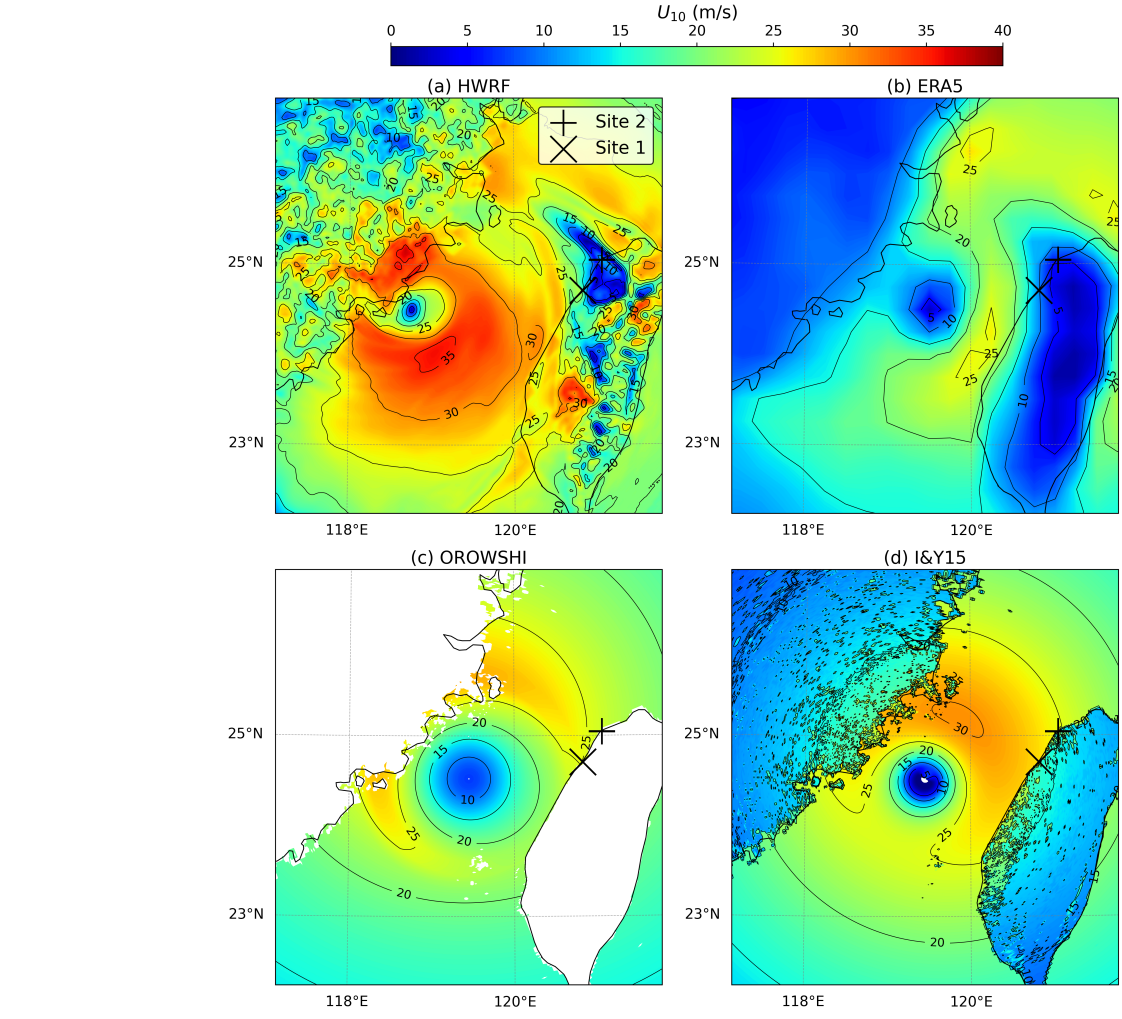

Figure 20. TC Megi surface wind field on 27 September at 6 P.M. GMT predicted by HWRF (a), ERA5 (b), OROWSHI wind model (c) and I&Y15 wind model (d).

Table 16. Mean absolute bias error (MABE) on V_m (2D).

Model	OROWSHI	I&Y15	ERA5	HWRF
MABE ($\mathrm{m.s^{-1}}$)	0.9	2.9	9.7	5.2

is consistent with the proposed formulation. This parameterisation enables efficient wind prediction at hub height and is more accurate than that recommended in the design standards for this dataset. The power law is also assessed as an alternative, the mean value derived from the measurement is 0.106.

https://doi.org/10.5194/wes-2025-273
Preprint. Discussion started: 16 December 2025

Furthermore, modelled time series of wind speeds are compared with measurements and high-fidelity model results from HWRF and ERA5. The wind model used in Ishihara and Yamaguchi (2015) is implemented for comparison. In general, the two parametric formulations perform as well as the high-fidelity models and show a fair agreement with the measurement, given the simplicity and the computational cost of these models. Scores such as MBE, RMSE and percent deviation on the maximum wind are computed for each event. In a design context where estimating the maximum wind speed is essential, the parametric models are more accurate than HWRF and ERA5. In particular, the OROWSHI model presents only a 5.1% mean absolute deviation from the maximum observed wind at sites, over twice as accurate as the other approaches. For its ease of implementation, computational cost and most importantly its ability to accurately predict the most severe winds induced by tropical cyclones, the model is suitable for implementation within a Monte Carlo framework to derive extreme wind statistics. Also, the surface wind fields are compared to discuss and analyse the differences between the models. The I&Y15 surface wind generally presents a broader eyewall than the OROWSHI model and HWRF results, which could lead to significant differences in terms of wave height estimates as wave models are forced with surface winds. The assessment of wind fields near large obstacles reveals the main limitation of the parametric models. These models, originally designed to represent tropical cyclones under ideal conditions, i.e. intense and over open ocean, tend to exhibit their largest errors when the cyclone deviates from this configuration. Landfalling TCs experience strong orographic effects that displace or attenuate wind maxima, leading to significant discrepancies with in-situ observations, as seen near Kyushu and Taiwan (Nanmadol, Megi). The magnitude of this landfall effect depends on coastline geometry and TC track. When the storm interacts with large obstacles, errors increase, particularly at sites exposed to offshore winds, already affected by land. Using parametric models instead of advanced dynamical models is therefore problematic for site-specific studies in regions with pronounced coastal orography. A minimal improvement would involve a site-adapted, more advanced parametrisation of asymmetry, accounting for variations in amplitude and azimuthal location based on the statistical properties at each site of interest.

Author contributions. PR: conceptualization, methodology, software, validation, data curation, investigation, writing (original draft), visualization, formal analysis. LV: conceptualization, software, methodology, writing (review and editing). FL: conceptualization, software, methodology, writing (review and editing) SU: conceptualization, methodology, writing (review and editing). JFF: conceptualization, methodology, supervision, writing (review and editing), project administration, funding acquisition

Competing interests. The authors declare that they have no known competing financial interests or personal relationships that could have appeared to influence the work reported in this paper.

Acknowledgements. This project receives funding from the FRANCE 2030 program, sponsored by the French government and implemented by the ANR, under the terms of Funding Allocation Agreement no. ANR-10-IEED-0006-34.

https://doi.org/10.5194/wes-2025-273
Preprint. Discussion started: 16 December 2025

eawe european academy of wind energy
Open Access WIND ENERGY SCIENCE DISCUSSIONS

References

Avenas, A., Mouche, A., Tandeo, P., Piolle, J.-F., Chavas, D., Fablet, R., Knaff, J., and Chapron, B.: Reexamining the Estimation of Tropical Cyclone Radius of Maximum Wind from Outer Size with an Extensive Synthetic Aperture Radar Dataset, Monthly Weather Review, 151, 3169 – 3189, https://doi.org/10.1175/MWR-D-23-0119.1, 2023.

Bell, M. M., Montgomery, M. T., and Emanuel, K. A.: Air–Sea Enthalpy and Momentum Exchange at Major Hurricane Wind Speeds Observed during CBLAST, Journal of the Atmospheric Sciences, 69, 3197 – 3222, https://doi.org/10.1175/JAS-D-11-0276.1, 2012.

Biswas, M.: Hurricane weather research and forecasting (HWRF) model: 2018 scientific documentation, 2018.

Bloemendaal, N., Haigh, I., Moel, H., Muis, S., Haarsma, R., and Aerts, J.: Generation of a global synthetic tropical cyclone hazard dataset using STORM, Scientific Data, 7, 40, https://doi.org/10.1038/s41597-020-0381-2, 2020.

Bouin, M.-N., Lebeaupin Brossier, C., Malardel, S., Voldoire, A., and Sauvage, C.: The wave-age-dependent stress parameterisation (WASP) for momentum and heat turbulent fluxes at sea in SURFEX v8.1, Geoscientific Model Development, 17, 117–141, https://doi.org/10.5194/gmd-17-117-2024, 2024.

British Standards Institution: Eurocode 1: Actions on structures – General actions – Part 1–4: Wind actions, European Committee for Standardization, Brussels, Belgium, 2005.

Bryant, M. and Akbar, M.: An Exploration of Wind Stress Calculation Techniques in Hurricane Storm Surge Modeling, Journal of Marine Science and Engineering, 4, https://doi.org/10.3390/jmse4030058, 2016.

Buchhorn, M., Smets, B., Bertels, L., Roo, B. D., Lesiv, M., Tsendbazar, N.-E., Herold, M., and Fritz, S.: Copernicus Global Land Service: Land Cover 100m: collection 3: epoch 2019: Globe, https://doi.org/10.5281/zenodo.3939050, 2020.

Chavas, D. and Knaff, J. A.: A Simple Model for Predicting the Tropical Cyclone Radius of Maximum Wind from Outer Size, Weather and Forecasting, 37, 563 – 579, https://doi.org/10.1175/WAF-D-21-0103.1, 2022.

DNV: Recommended Practice. DNV-RP-C205. Environmental Conditions and Environmental Loads, 2025.

Emanuel, K.: Response of Global Tropical Cyclone Activity to Increasing CO2: Results from Downscaling CMIP6 Models, Journal of Climate, 34, 57 – 70, https://doi.org/10.1175/JCLI-D-20-0367.1, 2021.

Emanuel, K., Ravela, S., Vivant, E., and Risi, C.: A Statistical Deterministic Approach to Hurricane Risk Assessment, Bulletin of the American Meteorological Society, 87, 299 – 314, https://doi.org/10.1175/BAMS-87-3-299, 2006.

Escalera, M., Griffith, D., Qin, C., Loth, E., and Johnson, N.: Rapid approach for structural design of the tower and monopile for a series of 25 MW offshore turbines, Journal of Physics Conference Series, 2265, 10, https://doi.org/10.1088/1742-6596/2265/3/032030, 2022.

Giammanco, I., Schroeder, J., and Powell, M.: Observed characteristics of tropical cyclone vertical wind profiles, Wind and Structures An International Journal, 15, 65–86, https://doi.org/10.12989/was.2012.15.1.065, 2012.

Grossmann-Matheson, G., Young, I., Alves, J.-H., and Meucci, A.: Development and validation of a parametric tropical cyclone wave height prediction model, Ocean Engineering, 283, 115 353, https://doi.org/10.1016/j.oceaneng.2023.115353, 2023.

Harper, B., Kepert, J., and Ginger, J.: Guidelines for Converting Between Various Wind Averaging Periods in Tropical Cyclone Conditions. World Meteorological Organization, 2010.

Hersbach, H., Bell, B., Berrisford, P., Biavati, G., Horányi, A., Muñoz Sabater, J., Nicolas, J., Peubey, C., Radu, R., Rozum, I., Schepers, D., Simmons, A., Soci, C., Dee, D., and Thépaut, J.-N.: ERA5 hourly data on single levels from 1940 to present, https://doi.org/10.24381/cds.adbb2d47, accessed on 24-07-2024, 2023.

https://doi.org/10.5194/wes-2025-273
Preprint. Discussion started: 16 December 2025

Holthuijsen, L., Powell, M., and Pietrzak, J.: Wind and waves in extreme hurricanes. J Geophys Res 117:C09003, Journal of Geophysical Research (Oceans), 117, https://doi.org/10.1029/2012JC007983, 2012.

Hsu, J.-H., Lien, R.-C.and D'Asaro, E., and Sanford, T.: Estimates of Surface Wind Stress and Drag Coefficients in Typhoon Megi, Journal of Physical Oceanography, 47, https://doi.org/10.1175/JPO-D-16-0069.1, 2017.

Hsu, L.-H., Su, S.-H., Fovell, R. G., and Kuo, H.-C.: On Typhoon Track Deflections near the East Coast of Taiwan, Monthly Weather Review, 146, 1495 – 1510, https://doi.org/10.1175/MWR-D-17-0208.1, 2018.

Hsu, S. A., Meindl, E. A., and Gilhousen, D. B.: Determining the power-law wind-profile exponent under near-neutral stability conditions at sea, Journal of Applied Meteorology, 33, 757–765, https://api.semanticscholar.org/CorpusID:120567835, 1994.

IEC: IEC 61400-1:2019 Wind energy generation systems - Part 1: Design requirements, 2019.

Ishihara, T. and Hibi, K.: Numerical study of turbulent wake flow behind a three-dimensional steep hill, Wind & Structures, 5, 317–328, 2002.

Ishihara, T. and Yamaguchi, A.: Prediction of the extreme wind speed in the mixed climate region by using Monte Carlo simulation and measure-correlate-predict method, Wind Energy, 18, 171–186, https://doi.org/https://doi.org/10.1002/we.1693, 2015.

Ishihara, T., Siang, K., Leong, C., and Fujino, Y.: Wind field model and mixed probability distribution function for typhoon simulation, in: The Sixth Asia-Pacific Conference on Wind Engineering (APCWE-VI), Seoul, Korea, 2005.

Janjic, Z.: The NCEP WRF core, Bulletin of the American Meteorological Society, 2004.

Kapoor, A., Ouakka, S., Arwade, S., Lundquiste, J., Lackner, M., Myers, A., Worsnop, R., and Bryan, G.: Hurricane eyewall winds and structural response of wind turbines, Wind Energy Science, 5, 89–104, https://doi.org/10.5194/wes-5-89-2020, 2020.

Kim, G. Y. and Lee, S.: Prediction of extreme wind by stochastic typhoon model considering climate change, Journal of Wind Engineering and Industrial Aerodynamics, 192, 17–30, https://doi.org/https://doi.org/10.1016/j.jweia.2019.05.003, 2019.

Knapp, K. R., Kruk, M. C., Levinson, D. H., Diamond, H. J., and Neumann, C. J.: The International Best Track Archive for Climate Stewardship (IBTrACS): Unifying Tropical Cyclone Data, Bulletin of the American Meteorological Society, 91, 363 – 376, https://doi.org/10.1175/2009BAMS2755.1, 2010.

Knapp, K. R., Diamond, H. J., Kossin, J. P., Kruk, M. C., and Schreck, C. J.: International Best Track Archive for Climate Stewardship (IBTrACS) Project, Version 4. NOAA National Centers for Environmental Information, https://doi.org/10.25921/82ty-9e16, 2023.

Knutson, T., Camargo, S. J., Chan, J. C. L., Emanuel, K., Ho, C.-H., Kossin, J., Mohapatra, M., Satoh, M., Sugi, M., Walsh, K., and Wu, L.: Tropical Cyclones and Climate Change Assessment: Part II: Projected Response to Anthropogenic Warming, Bulletin of the American Meteorological Society, 101, E303 – E322, https://doi.org/10.1175/BAMS-D-18-0194.1, 2020.

Larsén, X. G. and Ott, S.: Adjusted spectral correction method for calculating extreme winds in tropical-cyclone-affected water areas, Wind Energy Science, 7, 2457–2468, https://doi.org/10.5194/wes-7-2457-2022, 2022.

Liu, G., Jiang, S., Zheng, M., Lin, S., Kong, Y., and Zhan, P.: A Global ERA5-based Tropical Cyclone Wind Field Dataset Enhanced by Integrated Parametric Correction Methods, Sci Data, 12, https://doi.org/https://doi.org/10.1038/s41597-025-05789-w, 2025.

Loridan, T., Khare, S., Scherer, E., Dixon, M., and Bellone, E.: Parametric Modeling of Transitioning Cyclone Wind Fields for Risk Assessment Studies in the Western North Pacific, Journal of Applied Meteorology and Climatology, 54, 624 – 642, https://doi.org/10.1175/JAMC-D-14-0095.1, 2015.

Ma, X., Chen, Y., Yi, W., and Wang, Z.: Prediction of Extreme Wind Speed for Offshore Wind Farms Considering Parametrization of Surface Roughness, Energies, 14, https://doi.org/10.3390/en14041033, 2021.

https://doi.org/10.5194/wes-2025-273
Preprint. Discussion started: 16 December 2025

Meissner, T., Ricciardulli, L., and Wentz, F. J.: Capability of the SMAP Mission to Measure Ocean Surface Winds in Storms, Bulletin of the American Meteorological Society, 98, 1660 – 1677, https://doi.org/10.1175/BAMS-D-16-0052.1, 2017.

Meng, Y., Matsui, M., and Hibi, K.: An analytical model for simulation of the wind field in a typhoon boundary layer, Journal of Wind Engineering and Industrial Aerodynamics, 56, 291–310, https://doi.org/https://doi.org/10.1016/0167-6105(94)00014-5, 1995.

Meng, Y., Matsui, M., and Hibi, K.: A numerical study of the wind field in a typhoon boundary layer, Journal of Wind Engineering and Industrial Aerodynamics, 67-68, 437–448, https://doi.org/https://doi.org/10.1016/S0167-6105(97)00092-5, 1997.

Mouche, A., Chapron, B., Knaff, J., Zhao, Y., Zhang, B., and Combot, C.: Copolarized and Cross-Polarized SAR Measurements for High-Resolution Description of Major Hurricane Wind Structures: Application to Irma Category 5 Hurricane, Journal of Geophysical Research: Oceans, 124, 3905–3922, https://doi.org/https://doi.org/10.1029/2019JC015056, 2019.

Mudd, L. A. and Vickery, P. J.: Gulf of Mexico hurricane hazard assessment for offshore wind energy sites, Wind Energy Science, 10, 2685–2703, https://doi.org/10.5194/wes-10-2685-2025, 2025.

Müller, S., Guo Larsén, X., and Verelst, D.: Tropical cyclone low-level wind speed, shear, and veer: sensitivity to the boundary layer parametrization in the Weather Research and Forecasting model, Wind Energy Science, 9, 1153–1171, https://doi.org/10.5194/wes-9-1153-2024, 2024a.

Müller, S., Larsén, X., and Verelst, D.: Enhanced shear and veer in the Taiwan Strait during typhoon passage, Journal of Physics: Conference Series, 2767, 092 030, https://doi.org/10.1088/1742-6596/2767/9/092030, 2024b.

Olfateh, M., Callaghan, D. P., Nielsen, P., and Baldock, T. E.: Tropical cyclone wind field asymmetry—Development and evaluation of a new parametric model, Journal of Geophysical Research: Oceans, 122, 458–469, https://doi.org/https://doi.org/10.1002/2016JC012237, 2017.

Ott, S.: Extreme winds in the western North Pacific, Tech. Rep. Risoe-R-1544(EN), Risø National Laboratory, Roskilde, Denmark, https://orbit.dtu.dk/en/publications/extreme-winds-in-the-western-north-pacific, 2005.

Powell, M., Vickery, P., and Reinhold, T.: Reduced drag coefficient for high wind speeds in tropical cyclones, Nature, 20, 279–83, 2003.

Powell, M. D., Uhlhorn, E. W., and Kepert, J. D.: Estimating Maximum Surface Winds from Hurricane Reconnaissance Measurements, Weather and Forecasting, 24, 868 – 883, https://doi.org/10.1175/2008WAF2007087.1, 2009.

Reul, N., Chapron, B., Zabolotskikh, E., Donlon, C., Quilfen, Y., Guimbard, S., and Piolle, J.: A revised L-band radio-brightness sensitivity to extreme winds under Tropical Cyclones: the five year SMOS-storm database, Remote Sensing of Environment, 180, 274–291, https://doi.org/https://doi.org/10.1016/j.rse.2016.03.011, 2016.

Schloemer, R.: Analysis and synthesis of hurricane wind patterns over, Lake Okeechobee, Florida., Tech. rep., Hydrometeorogical Report, No.31, National Oceanic and Atmospheric Administration, 1954.

Simpson, R. H. and Saffir, H.: The hurricane disaster-potential scale, Weatherwise, 27, 169–186, https://doi.org/10.1080/00431672.1974.9931702, 1974.

Tamizi, A., Young, I. R., Ribal, A., and Alves, J.-H.: Global Scatterometer Observations of the Structure of Tropical Cyclone Wind Fields, Monthly Weather Review, 148, 4673 – 4692, https://doi.org/10.1175/MWR-D-20-0196.1, 2020.

Tan, C. and Fang, W.: Mapping the Wind Hazard of Global Tropical Cyclones with Parametric Wind Field Models by Considering the Effects of Local Factors, International Journal of Disaster Risk Science, 9, https://doi.org/10.1007/s13753-018-0161-1, 2018.

Tang, C. K. and Chan, J. C. L.: Idealized simulations of the effect of Taiwan topography on the tracks of tropical cyclones with different steering flow strengths, Quarterly Journal of the Royal Meteorological Society, 142, 3211–3221, https://doi.org/https://doi.org/10.1002/qj.2902, 2016.

https://doi.org/10.5194/wes-2025-273
Preprint. Discussion started: 16 December 2025

Türk, M., Grigutsch, K., and Emeis, S.: The Wind Profile Above the Sea-Investigations Basing on Four Years of FINO 1 Data, DEWI Magazine, 33, 12–16, 2008.

Vickery, P. J. and Twisdale, L. A.: Prediction of Hurricane Wind Speeds in the United States, Journal of Structural Engineering, 121, 1691–1699, https://doi.org/10.1061/(ASCE)0733-9445(1995)121:11(1691), 1995.

Vickery, P. J., Skerlj, P. F., and Twisdale, L. A.: Simulation of Hurricane Risk in the U.S. Using Empirical Track Model, Journal of Structural Engineering, 126, 1222–1237, https://doi.org/10.1061/(ASCE)0733-9445(2000)126:10(1222), 2000.

Vickery, P. J., Wadhera, D., Powell, M. D., and Chen, Y.: A Hurricane Boundary Layer and Wind Field Model for Use in Engineering Applications, Journal of Applied Meteorology and Climatology, 48, 381 – 405, https://doi.org/10.1175/2008JAMC1841.1, 2009.

Vinour, L., Jullien, S., Mouche, A., and Avenas, A.: Review and Improvement of Tropical Cyclone Surface Wind Parametric Models Using SAR Imagery, Submitted to Journal of Applied Meteorology and Climatology, 2025.

Wang, J., Tse, K., Li, S., and Fung, J.: Prediction of the typhoon wind field in Hong Kong: integrating the effects of climate change using the Shared Socioeconomic Pathways, Climate Dynamics, 59, https://doi.org/10.1007/s00382-022-06211-6, 2022.

Willoughby, H. E. and Rahn, M. E.: Parametric Representation of the Primary Hurricane Vortex. Part I: Observations and Evaluation of the Holland (1980) Model, Monthly Weather Review, 132, 3033 – 3048, https://doi.org/10.1175/MWR2831.1, 2004.

Wu, C.-C., Li, T.-H., and Huang, Y.-H.: Influence of Mesoscale Topography on Tropical Cyclone Tracks: Further Examination of the Channeling Effect, Journal of the Atmospheric Sciences, 72, 3032 – 3050, https://doi.org/10.1175/JAS-D-14-0168.1, 2015.

Xu, Z., Guo, J., Zhang, G., Ye, Y., Zhao, H., and Chen, H.: Global tropical cyclone size and intensity reconstruction dataset for 1959–2022 based on IBTrACS and ERA5 data, Earth System Science Data, 16, 5753–5766, https://doi.org/10.5194/essd-16-5753-2024, 2024.

Yamaguchi, A., Solomon, M., and Ishihara, T.: An effect of the averaging time on maximum mean wind speeds during tropical cyclone, in: The European Wind Energy Conference and Exhibition 2012, 2012.

Yan, B., Li, Q., Chan, P., He, Y., and Shu, Z.: Characterising wind shear exponents in the offshore area using Lidar measurements, Applied Ocean Research, 127, 103 293, https://doi.org/https://doi.org/10.1016/j.apor.2022.103293, 2022.

Yan, D. and Zhang, T.: Research progress on tropical cyclone parametric wind field models and their application, Regional Studies in Marine Science, 51, 102 207, https://doi.org/https://doi.org/10.1016/j.rsma.2022.102207, 2022.

Yasui, H., Ohkuma, T., Marukawa, H., and Katagiri, J.: Study on evaluation time in typhoon simulation based on Monte Carlo method, Journal of Wind Engineering and Industrial Aerodynamics, 90, 1529–1540, https://doi.org/https://doi.org/10.1016/S0167-6105(02)00268-4, fifth Asia-Pacific Conference on Wind Engineering, 2002.

Zhang, J. A. and Uhlhorn, E. W.: Hurricane Sea Surface Inflow Angle and an Observation-Based Parametric Model, Monthly Weather Review, 140, 3587 – 3605, https://doi.org/10.1175/MWR-D-11-00339.1, 2012.

Zijlema, M., van Vledder, G., and Holthuijsen, L.: Bottom friction and wind drag for wave models, Coastal Engineering, 65, 19–26, https://doi.org/https://doi.org/10.1016/j.coastaleng.2012.03.002, 2012.